NASA Technical Paper 1133

Inviscid, Nonadiabatic Flow Fields Over Blunt, Sonic Corner Bodies for Outer Planet Entry Conditions by a Method of Integral Relations

Peter A. Gnoffo

FEBRUARY 1978

NASA

NASA Technical Paper 1133

Inviscid, Nonadiabatic Flow Fields Over Blunt, Sonic Corner Bodies for Outer Planet Entry Conditions by a Method of Integral Relations

Peter A. Gnoffo
Langley Research Center
Hampton, Virginia

National Aeronautics
and Space Administration

**Scientific and Technical
Information Office**

1978

SUMMARY

An investigation has been made into the ability of a method of integral relations to calculate inviscid, 0^{o} angle of attack, radiative heating distributions over blunt, sonic corner bodies for some representative outer planet entry conditions. Comparisons have been made with a more detailed numerical method, a time asymptotic technique, using the same equilibrium chemistry and radiation transport subroutines. An effort to produce a second-order approximation (two-strip) method of integral relations code to aid in this investigation is also described and a modified two-strip routine is presented. Results indicate that the one-strip method of integral relations cannot be used to obtain accurate estimates of the radiative heating distribution because of its inability to resolve thermal gradients near the wall. The two-strip method can sometimes be used to improve these estimates; however, the two-strip method has only a small range of conditions over which it will yield significant improvement over the one-strip method.

INTRODUCTION

The method of integral relations is a numerical procedure which has been used by many researchers to obtain inviscid shock layer solution around blunt bodies in supersonic flow. (See refs. 1 to 6.) The single-strip method runs rapidly on the computer and gives results which are within engineering accuracy for most applications to adiabatic flow situations. Applications of this method to nonadiabatic flow situations involving radiative heat transfer have been investigated by Suttles (ref. 1) and Edquist (ref. 2). Suttles studied the nonadiabatic flow over two spheres in equilibrium air by using a one-strip integral method but there were no detailed comparisons available with other numerical methods. Radiative heating contributions were fully coupled with the other flow equations in that report. Edquist also used a one-strip method to compute equilibrium gas flow over spherically capped cones with sonic corners. The radiative heating contributions in that study were not directly coupled to the governing flow equations and no detailed comparisons were presented with other solution techniques.

The purpose of this report is to make a detailed comparison of the method of integral relations (designated MIR) with a more exact numerical method, the time asymptotic technique (designated TAT) (ref. 7). Radiative heating contributions are fully coupled with the fluid mechanics in this investigation. The merits of MIR as a tool for making radiative heating calculation over blunt, sonic corner bodies are evaluated.

There are two major reasons for an interest in this type of investigation. Exploratory missions to the outer planets by instrumented probe vehicles are tentatively scheduled for the next decade. The entry environment experienced by these probes must be understood in sufficient detail to be able to perform atmospheric reconstruction analyses and to insure their survival during a severe

heating-deceleration pulse. The TAT is currently used for making these calculations, but it would be advantageous if a faster running MIR could be implemented to replace or supplement that method.

Also, recent investigations into shape changes caused by massive ablation during entry into the Jupiter atmosphere have indicated the possibility of producing forebody concavities (ref. 8) which cannot be analyzed by TAT as it is now formulated. The ability of MIR to calculate flow over bodies with concavities has already been demonstrated by South (ref. 3) and Rao (ref. 4). However, before MIR is used for these studies, the consequences of the cruder approximations inherent in the method should be understood. To this end, this study is restricted to the solution of problems which are characteristic of planetary probes entering hydrogen-helium atmospheres.

It should also be noted that during the course of this investigation, some time was spent in the development of a higher order (two-strip) MIR. A summary of the results of this development is presented along with some two-strip MIR flow field solutions for inviscid, adiabatic, and nonadiabatic flow over blunt, spherically capped cones.

SYMBOLS

A,B,C,D,E,F	nondimensional constants defined in equations (A3) to (A8)
a	speed of sound, a^*/V_∞^*
C_H,C_{He}	mass fraction of hydrogen and helium, respectively
$C_1,C_2,\ldots,C_9$	nondimensional constants defined in equations (12)
C_2',C_3',C_8',C_9'	nondimensional constants defined in equations (17)
D	damping factor
$G_1,G_2,\ldots,G_5$	nondimensional functions of p, ρ, u, v, and H defined in equations (2)
H	total enthalpy, H^*/V_∞^{*2}
h	static enthalpy, h^*/V_∞^{*2}
$I_1,I_2,\ldots,I_5$	nondimensional functions of p, ρ, u, v, H, δ, and r defined in equations (2)
K	strip index
$L_1,L_2,\ldots,L_5$	nondimensional functions of p, ρ, u, v, H, δ, Q, ω, θ_b, r, η, and s defined in equations (2)
M	Mach number

M_∞	free-stream Mach number, V_∞^*/a_∞^*
N	number of strips
p	pressure, $p^*/\rho_\infty^* V_\infty^{*2}$
Q	curvature of reference surface, R_N^*/R_b^*
q_R	radiative heat flux, $q_R^*/\rho_\infty^* V_\infty^{*3}$
R	radius of curvature, R^*/R_N^*
R_g^*	gas constant, $m^2/(s^2\text{-}K)$
r	radius from axis of symmetry, r^*/R_N^*
s,y	body-oriented coordinates (see fig. 1), s^*/R_N^*, y^*/R_N^*
T^*	temperature, K
u	tangential velocity, u^*/V_∞^*
V_∞^*	free-stream velocity, m/s
v	normal velocity, v^*/V_∞^*
x,z	Cartesian coordinates
γ	ratio of specific heats
δ	shock displacement distance, δ^*/R_N^*
η	transformed y coordinate, y/δ
θ_b	body angle, deg
θ_c	cone angle, deg
κ	metric coefficient, $1 + Q\delta\eta$
ρ	density, ρ^*/ρ_∞^*
ω	shock angle, deg

Superscripts:

n	iteration number
*	dimensional quantity
~	undamped quantity

'	converged value of iterative variable on stagnation line

Subscripts:

B	base
b	local body conditions
j	refers to particular governing differential equation: j = 1; shock geometry equation j = 2; continuity equation j = 3; s-momentum equation j = 4; y-momentum equation j = 5; energy equation
K0	refers to conditions on lower boundary (body side) of kth strip
K1	refers to conditions on upper boundary (shock side) of kth strip
N	nose
R	radiative
s	shock
stag	stagnation point conditions
∞	free-stream conditions

Abbreviations:

MIR	method of integral relations
TAT	time asymptotic technique

ANALYSIS

The application of the integral method and the derivation of the approximating system of nonlinear ordinary differential equations closely follows the development presented in reference 6. However, an Nth order approximation is considered herein which involves the construction of N parallel computational strips between the body and the shock. This construction of parallel strips corresponds to scheme I of the method of integral relations (MIR) as described by Belotserkovskiy (ref. 5). For N = 1, the equations which follow will reduce to the equations in reference 6.

Governing Equations

The conservation equations for the steady axisymmetric flow of an inviscid radiating gas written in a body-oriented coordinate system are (from ref. 6)

$$\frac{\partial(I_j r)}{\partial s} - \frac{\eta}{\delta}\frac{d\delta}{ds}\frac{\partial(I_j r)}{\partial \eta} + \frac{1}{\delta}\frac{\partial(G_j \kappa r)}{\partial \eta} + L_j = 0 \tag{1}$$

where

$$\left.\begin{aligned}
&\eta = \frac{y}{\delta} \qquad \text{and} \qquad \delta = \delta(s) \\
&I_1 = \frac{\delta}{r} \qquad G_1 = 0 \qquad L_1 = -(1 + Q\delta)\tan(\omega - \theta_b) \\
&I_2 = \rho u \qquad G_2 = \rho v \qquad L_2 = 0 \\
&I_3 = p + \rho u^2 \qquad G_3 = \rho uv \qquad L_3 = -\left(\frac{dr_b}{ds} - \delta\eta \sin\theta_b \frac{d\theta_b}{ds}\right)p + Qr I_4 \\
&I_4 = \rho uv \qquad G_4 = p + \rho v^2 \qquad L_4 = -(Qr + \kappa\cos\theta_b)p - Qr\rho u^2 \\
&I_5 = \rho uH \qquad G_5 = \rho vH \qquad L_5 = \frac{1}{\delta}\frac{\partial}{\partial \eta}(\kappa r q_R)
\end{aligned}\right\} \tag{2}$$

The relationship between the shock and the body geometry in a body-oriented coordinate system is governed by equation (1) with $j = 1$ (ref. 6).

The relation for L_5 has been established by making the local tangent slab approximation so that from reference 6,

$$q_{Rs} = \frac{\partial}{\partial s}(q_R) = 0$$

$$q_R = q_{Ry}$$

The coordinate system is presented in figure 1. All these quantities have been nondimensionalized as follows:

$$\left.\begin{aligned}
&y = \frac{y^*}{R_N^*} \qquad v = \frac{v^*}{V_\infty^*} \qquad u = \frac{u^*}{V_\infty^*} \qquad \rho = \frac{\rho^*}{\rho_\infty^*} \\
&\delta = \frac{\delta^*}{R_N^*} \qquad R_b = \frac{R_b^*}{R_N^*} \qquad r = \frac{r^*}{R_N^*} \qquad p = \frac{p^*}{\rho_\infty^*(V_\infty^*)^2} \\
&s = \frac{s^*}{R_N^*} \qquad Q = Q^* R_N^* \qquad q_R = \frac{q_R^*}{\rho_\infty^*(V_\infty^*)^3} \qquad H = \frac{H^*}{(V_\infty^*)^2}
\end{aligned}\right\} \tag{3}$$

In addition to equation (1) relationships for $p = p(\rho, h)$ and for q_{Ry} as a function of thermodynamic properties across the shock layer are required and are presented in later sections.

Application of MIR

In figure 1 the computational field in the s,η coordinate system is shown divided into N strips of equal width. Each strip is indexed by an integer K where $K = 1$ for the strip bounding the body and $K = N$ for the strip adjacent to the shock. The following linear approximations across each individual strip are assumed:

$$\left.\begin{aligned} I_j(\eta) &= (I_j)_{K1} + \left[(I_j)_{K1} - (I_j)_{K0}\right](N\eta - K) \\ p(\eta) &= p_{K1} + (p_{K1} - p_{K0})(N\eta - K) \end{aligned}\right\} \tag{4}$$

where

$$\frac{K-1}{N} \leqq \eta \leqq \frac{K}{N}$$

$$K = 1,2,\ldots,N$$

$$j = 2,3,4,5$$

and the I_j are defined in equations (2). The subscript $K0$ refers to conditions on the bottom boundary of the Kth strip and $K1$ refers to conditions on the top boundary of the Kth strip. At any given s location it can be shown that $(I_j)_{K1} = (I_j)_{(K+1)0}$ and $p_{K1} = p_{(K+1)0}$ for $K + 1 = 2,3,\ldots,N$.

Multiplying equation (1) by δ and integrating the result with respect to η across the Kth strip yields

$$\delta \int_{(K-1)/N}^{K/N} \frac{\partial(I_j r)}{\partial s}\, d\eta - \frac{d\delta}{ds} \int_{(K-1)/N}^{K/N} \eta \frac{\partial(I_j r)}{\partial \eta}\, d\eta + \int_{(K-1)/N}^{K/N} \frac{\partial(G_{jK} r)}{\partial \eta}\, d\eta$$

$$+ \int_{(K-1)/N}^{K/N} L_j\, d\eta = 0 \qquad (j = 2,3,4,5) \tag{5}$$

Equation (5) is simplified by applying Leibniz's rule to the first term, by integrating the second term by parts, and by directly integrating the third term. The resulting equation is

$$\delta \frac{d}{ds}\left(\int_{(K-1)/N}^{K/N} I_j r\, d\eta\right) - \frac{d\delta}{ds}\left[(\eta I_j r)\Big|_{(K-1)/N}^{K/N} - \int_{(K-1)/N}^{K/N} I_j r\, d\eta\right] + (G_{jK} r)\Big|_{(K-1)/N}^{K/N}$$

$$+ \int_{(K-1)/N}^{K/N} L_j\, d\eta = 0 \tag{6}$$

The remaining integrals are evaluated by substituting the linear relationships from equations (4) and (7)

$$\left.\begin{aligned} r &= r_b + \eta\delta \cos\theta_b \\ \kappa &= 1 + Qy = 1 + Q\delta\eta \end{aligned}\right\} \tag{7}$$

After further algebraic manipulation, the transformed governing equations are written:

Continuity:

$$C_1\left[(\rho u)_{K0} - (\rho u)_{K1}\right] + C_2(\rho v)_{K1} + C_3(\rho v)_{K0} + C_4(\rho u)_{K0} + C_5(\rho u)_{K1}$$

$$+ C_6 \frac{d(\rho u)_{K0}}{ds} + C_7 \frac{d(\rho u)_{K1}}{ds} = 0 \tag{8}$$

Normal momentum:

$$C_1\left[(\rho uv)_{K0} - (\rho uv)_{K1}\right] + C_2(p + \rho v^2)_{K1} + C_3(p + \rho v^2)_{K0} + C_4(\rho uv)_{K0}$$

$$+ C_5(\rho uv)_{K1} + C_6\left[\frac{d(\rho uv)_{K0}}{ds} - Q(p + \rho u^2)_{K0}\right] + C_7\left[\frac{d(\rho uv)_{K1}}{ds} - Q(p + \rho u^2)_{K1}\right]$$

$$+ C_8 p_{K0} + C_9 p_{K1} = 0 \tag{9}$$

Tangential momentum:

$$C_1\left[(p + \rho u^2)_{K0} - (p + \rho u^2)_{K1}\right] + C_2(\rho uv)_{K1} + C_3(\rho uv)_{K0} + C_4(\rho u^2)_{K0} + C_5(\rho u^2)_{K1}$$

$$+ C_6\left[\frac{d(p + \rho u^2)_{K0}}{ds} + Q(\rho uv)_{K0}\right] + C_7\left[\frac{d(p + \rho u^2)_{K1}}{ds} + Q(\rho uv)_{K1}\right] = 0 \tag{10}$$

Energy:

$$C_1\left[(\rho uH)_{K0} - (\rho uH)_{K1}\right] + C_2(\rho vH + q_R)_{K1} + C_3(\rho vH + q_R)_{K0} + C_4(\rho uH)_{K0} + C_5(\rho uH)_{K1}$$

$$+ C_6 \frac{d(\rho uH)_{K0}}{ds} + C_7 \frac{d(\rho uH)_{K1}}{ds} = 0 \tag{11}$$

where

$$
\left.
\begin{aligned}
C_1 &= \left[3N(2K-1)r_b + 2(3K^2 - 3K + 1)\delta \cos\theta_b\right]\frac{d\delta}{ds} \\
C_2 &= 6N^2\left(1 + Q\delta\,\frac{K}{N}\right)\left(r_b + \delta\,\frac{K}{N}\cos\theta_b\right) \\
C_3 &= -6N^2\left(1 + Q\delta\,\frac{K-1}{N}\right)\left(r_b + \delta\,\frac{K-1}{N}\cos\theta_b\right) \\
C_4 &= \delta\left[3N\,\frac{dr_b}{ds} - (3K-2)\delta\sin\theta_b\,\frac{d\theta_b}{ds}\right] \\
C_5 &= \delta\left[3N\,\frac{dr_b}{ds} - (3K-1)\delta\sin\theta_b\,\frac{d\theta_b}{ds}\right] \\
C_6 &= \delta\left[3Nr_b + (3K-2)\delta\cos\theta_b\right] \\
C_7 &= \delta\left[3Nr_b + (3K-1)\delta\cos\theta_b\right] \\
C_8 &= -\delta\cos\theta_b\left[3N + (3K-2)\delta Q\right] \\
C_9 &= -\delta\cos\theta_b\left[3N + (3K-1)\delta Q\right]
\end{aligned}
\right\} \qquad (12)
$$

It has been noted (ref. 6) that numerical instabilities can be eliminated for $N = 1$ if the integrated form of the tangential momentum equation (eq. (10)) is replaced by the exact form of the tangential momentum equation on the body.

The exact form of the tangential momentum equation on the body can be obtained from combining equation (1) ($j = 2$) with equation (1) ($j = 3$) while noting that $\eta = 0$ and $v = 0$ to yield

$$
\frac{d(I_3)_{1,0}}{ds} - u_{1,0}\,\frac{d(I_2)_{1,0}}{ds} = 0 \qquad (13)
$$

When $K = 1$, equation (13) replaces equation (10).

Solution Procedure

Overview.- The ordinary differential equations (eqs. (8) to (10) and (13)) are numerically integrated around the body from the axis of symmetry (for 0° angle of attack), adiabatic flow being assumed ($H = H_{\infty}$). The limiting forms of the governing equations are obtained on the axis of symmetry and it is found that for N strips, there are N more unknowns than equations. The N additional relations required on the axis of symmetry are obtained from regularity conditions on the sonic line and a sonic corner condition which must be satisfied downstream. Consequently, the solution procedure is similar to a shooting method for a two-point boundary value problem, in which N initial conditions on the axis of symmetry must be iteratively adjusted until $N - 1$ regularity conditions and a sonic corner condition ($M_{10} = 1.0$) are satisfied downstream on the sonic line.

For $N = 1$, the shock standoff distance δ_{stag} is the initial condition which is iteratively adjusted to force $M = 1.0$ at the sonic corner. For $N > 1$, the velocities at the boundaries of adjacent strips are also iteratively adjusted so that the governing equations can be integrated across the saddle point singularity located on the sonic line. (A description of the saddle point singularity and the behavior of the governing equations near the singularity are presented in refs. 3, 5, and 6.)

A fully converged adiabatic solution is obtained when all downstream regularity conditions and the sonic corner condition are satisfied by using the adjusted iterative variables at $s = 0$ for initial conditions. The thermodynamic conditions around the body are saved and radiative heat fluxes are calculated and saved for use in the energy equation. Equations (8) to (11) and (13) are now numerically integrated around the body from the axis of symmetry (by using the updated values of the radiative heat fluxes) and a new set of initial conditions must be obtained. When a converged solution is obtained by using the old values of radiative heat fluxes, new values for the radiative heat fluxes can be calculated by using the updated thermodynamic distributions. Thus, there are two iterative procedures involved in obtaining a converged nonadiabatic solution. The first procedure (Procedure I) involves an iterative process on the initial conditions to obtain a solution around the body while holding the radiative heat flux distribution unchanged (even though thermodynamic distributions are changing during the process). The second procedure (Procedure II) involves the process whereby the radiative heat fluxes are updated everywhere in the field after which program control is passed back to Procedure I. As program control alternates between Procedure I and Procedure II, changes in the radiative heating distribution go to zero and convergence is achieved.

Initial conditions.- The transformed system of governing equations includes $4N$ ordinary differential equations (eqs. (8) to (11) and (13)), which are indeterminant at $s = 0$. The limiting forms of these equations are obtained by differentiating them with respect to s. However, all the terms in the tangential momentum equations vanish quadratically at $s = 0$; thus, a single differentia-

tion does not remove the indeterminacy. One can either differentiate the tangential momentum equations again with respect to s and solve for d^2p/ds^2 along the symmetry line on the strip boundaries or ignore the tangential momentum equations on the symmetry line. The first approach ultimately requires a specification of d^2p/ds^2 on the stagnation point whereas the second approach only requires a specification of p on the stagnation point. Because d^2p/ds^2 could not be adequately specified for many different body shapes, the second approach (ignoring tangential momentum on the symmetry line) was implemented.

The limiting form of the governing equations on the symmetry line are:

Continuity:

$$C_2'(\rho v)_{K1} + C_3'(\rho v)_{K0} + 2C_4\left(\rho \frac{du}{ds}\right)_{K0} + 2C_5\left(\rho \frac{du}{ds}\right)_{K1} = 0 \tag{14}$$

Normal momentum:

$$C_2'(p + \rho v^2)_{K1} + C_3'(p + \rho v^2)_{K0} + 2C_4\left(\rho v \frac{du}{ds}\right)_{K0} + 2C_5\left(\rho v \frac{du}{ds}\right)_{K1} - C_4 Q p_{K0}$$

$$- C_5 Q p_{K1} + C_8' p_{K0} + C_9' p_{K1} = 0 \tag{15}$$

Energy:

$$C_2'(\rho v H + q_R)_{K1} + C_3'(\rho v H + q_R)_{K0} + 2C_4\left(\rho H \frac{du}{ds}\right)_{K0} + 2C_5\left(\rho H \frac{du}{ds}\right)_{K1} = 0 \tag{16}$$

where

$$\left.\begin{aligned}
C_2' &= 6N^2\left(1 + Q\delta_{stag}\frac{K}{N}\right)\left(\frac{dr_b}{ds} - \delta_{stag}\frac{d\theta_b}{ds}\frac{K}{N}\right) \\
C_3' &= -6N^2\left(1 + Q\delta_{stag}\frac{K-1}{N}\right)\left(\frac{dr_b}{ds} - \delta_{stag}\frac{d\theta_b}{ds}\frac{K-1}{N}\right) \\
C_8' &= \delta_{stag}\frac{d\theta_b}{ds}\left[3N + (3K-2)\delta_{stag}Q\right] \\
C_9' &= \delta_{stag}\frac{d\theta_b}{ds}\left[3N + (3K-1)\delta_{stag}Q\right]
\end{aligned}\right\} \tag{17}$$

The unknowns in equations (14) to (16) are

Unknown	Number of unknowns
$\rho_{10}, \rho_{20}, \ldots, \rho_{N0}, \rho_{N1}$	N + 1
$v_{10}, v_{20}, \ldots, v_{N0}, v_{N1}$	N + 1
$du_{10}/ds, du_{20}/ds, \ldots, du_{N0}/ds, du_{N1}/ds$	N + 1
$q_{R10}, q_{R20}, \ldots, q_{RN0}, q_{RN1}$	N + 1
$H_{10}, H_{20}, \ldots, H_{N0}, H_{N1}$	N + 1
$p_{10}, p_{20}, \ldots, p_{N0}, p_{N1}$	N + 1
δ_{stag}	1

The variable H_{N1} is equal to H_∞ from conservation of energy across a shock. (For adiabatic flow H is a constant equal to H_∞ and equation (16) is redundant.) Values of $q_{R10}, q_{R20}, \ldots, q_{RN0}$, and q_{RN1} are equal to zero for an adiabatic solution and are calculated from thermodynamic data on the stagnation line (obtained from Procedure I) by using a tangent slab approximation for nonadiabatic solutions. Note also that $v_{10} = 0$ (no mass flux through body) and that the stagnation pressure p_{10} can be approximated as (ref. 6)

$$p_{10} = p_s + \frac{1}{2}\rho_s v_s^2$$

In addition, there are N + 1 local equations of state (see appendix) relating pressure to density and enthalpy on the strip boundaries. There are also two more equations (Rankine-Hugoniot relations) governing the conservation of mass and momentum across a normal shock. Consequently, there are a total of 4N + 3 equations and 5N + 3 unknowns. The N additional relations required come from regularity conditions on N - 1 strip boundaries between the body and the shock which must be enforced on the sonic line and the imposition of a Mach number of 1.0 at the aft corner of the body. There are N unknowns ($\delta_{stag}, v_{20}, v_{30}, \ldots$, and v_{N0}) which must be guessed at initially and iteratively corrected until all N conditions are satisfied simultaneously (Procedure I).

This procedure is most easily implemented for N = 1 where, in the sonic corner problem, only one variable is iterated to force a Mach 1.0 condition at the aft corner of the body. If the Mach number M_{10} is greater than 1.0 before the corner or if the solution to the governing equations will not converge at some downstream location (see next section), δ_{stag} is increased. If the Mach number is less than 1.0 at the aft corner of the body, δ_{stag} is decreased.

Solution of governing equations downstream of symmetry line.- The derivatives in equations (8) to (11) and (13) are calculated by using three-point backward finite-difference formulas. For example,

$$\left.\frac{d\rho u}{ds}\right|_{10} = C_1\rho u_{10}(s) + C_2\rho u_{10}(s - \Delta s_1) + C_3\rho u_{10}(s - \Delta s_1 - \Delta s_2)$$

where

$$C_1 = (1 + 2f)/[f\ \Delta s_2(1 + f)]$$

$$C_2 = -(1 + f)/(f\ \Delta s_2)$$

$$C_3 = f/[\Delta s_2(1 + f)]$$

$$f = \Delta s_1/\Delta s_2$$

Δs_1 current increment in s

Δs_2 previous increment in s

The conservation equations, coupled with the local equations of state (appendix A), the Rankine-Hugoniot relations (ref. 6), and the shock geometry relation (from eq. (1), $j = 1$)

$$\frac{d\delta}{ds} - (1 + Q\delta)\tan(\omega - \theta_b) = 0 \qquad (18)$$

now form a system of $5N + 5$ nonlinear, algebraic equations with $5N + 5$ unknowns. These algebraic equations are solved at every integration step by using a quadratically convergent Newton-Raphson technique. For the case of adiabatic flow, H is a known constant and the energy equations can be replaced; thus, a system of $4N + 5$ equations with $4N + 5$ unknowns remains. The equations are solved at a given s location, an increment Δs is chosen, and the procedure is repeated at a new body station until the sonic corner is reached or the Newton-Raphson technique fails. (This failure occurs because the system of equations becomes ill-conditioned.) At this point the initial conditions are adjusted and the entire solution procedure is repeated until all the regularity conditions on the sonic line are met and the Mach number at the aft corner of the body is equal to 1.0.

Radiative heating calculations.- The coupling of the radiative heat flux in the energy equation is accomplished in an iterative manner (Procedure II). An adiabatic solution is obtained and the thermodynamic state at each computational point is saved. The radiative heat flux along a ray normal to the body is calculated from these data by using the tangent slab approximation as utilized in subroutine RAD/EQUIL (ref. 9). Within RAD/EQUIL, line and continuum radiation are included. The radiative heat fluxes on the strip boundaries are stored and used in the energy equation to compute an approximation to the nonadiabatic solution. A new thermodynamic state from the latest nonadiabatic solution is

used to compute new radiative heat flux distributions. This successive substitution process is continued until

$$\left| \frac{q_{R,stag}^{n} - q_{R,stag}^{n-1}}{q_{R,stag}^{n}} \right| < 0.0005$$

Values of q_R away from the stagnation point can have larger differences between iterations but it was found that the convergence criteria specified at the stagnation point will result in all variables being converged to within three significant figures. A flow chart of the entire solution procedure is presented in figure 2.

In some cases with strong radiative heating, it was found necessary to damp the calculated radiative heat flux when substituting into the energy equation. Thus, it would be specified that

$$q_R^n = D\tilde{q}_R^n + (1 - D)q_R^{n-1}$$

where $D = 0.75$ would usually be a sufficient damping factor. For all the cases considered, the convergence criterion for the nonadiabatic solution was usually satisfied after five to seven successive substitutions.

Two-Strip Solutions

From a practical point of view, MIR is limited to a one-strip solution ($N = 1$). The complexity of the iteration procedure makes multistrip solutions very difficult to obtain. The problems of a multistrip approach to the method of integral relations can be summarized as follows by using a two-strip approximation with equally spaced strips as an example.

In the two-strip approximation, there are two initial conditions on the stagnation line which must be specified: δ_{stag}, the shock standoff distance, and v_{20}, the velocity on the strip boundary between the body and the shock. A solution is obtained when the governing equations can be integrated along each strip to a line normal to the aft corner of the body with a Mach number of 1.0 at the corner. For the conditions illustrated in figure 3, the equations must be integrated across the sonic line. The position of the sonic line in the flow field gives an indication of the location of singular points of the governing equations (ref. 5). The iterative variable δ_{stag} and v_{20} must be adjusted to a precision fine enough to simultaneously allow the governing equations to be integrated through a singularity in the transonic region of the flow field and to force the Mach number condition at the corner.

In reference 6, it was reported that about four figure accuracy in δ_{stag} is necessary to integrate through the transonic region of a sphere using a one-strip MIR. It was also reported that there was poor agreement with experimental data in the transonic and low supersonic regions because no criteria can be established to guide further refinement of δ_{stag} to improve the solution. In the flow field depicted in figure 3, much of the region above the cone flank

can be classified as transonic and low supersonic. Therefore, in a two-strip procedure, one should expect some difficulty in using MIR since the upper strip will pass through a long region of transonic and low supersonic flow.

Many of the difficulties associated with a two-strip MIR can be overcome if the flow field surrounding the body is characterized by a sonic line which lies very close to the downstream boundary of the computational domain (fig. 4). Such flows can be found on very wide angle bodies although the details of the location of the sonic line are also Mach number and γ dependent. A two-strip solution procedure with equally spaced strips was successfully implemented for flows exhibiting this type of behavior in helium ($\gamma = 1.67$). The criteria for obtaining a solution can be summed up as follows:

(1) $M_{10} = 1 \pm 0.01$ on aft corner of body

(2) Shock angle ω is monotonically decreasing

(3) $v_{20}(s) < 0$

The iterative variable δ_{stag} is held constant and the variable v_{20} is iterated according to the criteria described. If $\frac{v_{20}^{n} - v_{20}^{n-1}}{v_{20}^{n}} < 10^{-8}$, where the superscript n indicates the nth iteration, and all of the solution criteria have not been met, then δ_{stag} is adjusted and the iteration on v_{20} is implemented again. The procedure is continued until all the solution criteria are met. A sample calculation is presented in figure 5 with comparisons to experimental data from reference 10 that use this approach.

However, there are still some problems with this approach. The execution time for this program on the computer is significantly increased because it involves a double iteration procedure and because a smaller integration step size (as compared with the one-strip MIR) is required to maintain stability. The solution procedure is not closed. There is a small range of values for δ_{stag} and v_{20} which can be used that satisfy the solution criteria. In the small number of cases tested, this relationship between δ_{stag} and v_{20} is linear (fig. 6). The final problem is that the iteration procedure will only work for values of δ_{stag} and v_{20} close to the true solution. A one-strip solution must be obtained to determine an approximate value for δ_{stag} to be used in the two-strip solution. Then a range of values for v_{20} must be determined so that the solution can be integrated far enough downstream to insure that the criteria for adjustments on v_{20} are still valid.

Typically, values for v_{20} differing by 5 percent from v_{20}' could be iterated to obtain a solution to the problem. (The quantities v_{20}' and δ_{stag}' are the values of v_{20} and δ_{stag} which satisfy all the convergence criteria.) Values of v_{20} differing by more than ± 5 percent from v_{20}' would cause the solution to diverge before the sphere-cone junction and no clear reason for this divergence was observed. In many cases, this divergence was manifested by the fact that the Newton-Raphson solution of the governing system of nonlinear algebraic equations would fail to converge to any solution near the stagnation line. (Other two-strip solutions have been reported by

Belotserkovskiy (ref. 5), Inouye and Marvin (ref. 11), and Holt and Hoffman (ref. 12). The complexity of the iteration procedure and the increased computer time required for mathematically closed two-strip solutions have caused most researchers using the method of integral relations to concentrate on obtaining as much information as possible by using the relatively simple one-strip approach.)

For wide-angle bodies where the sonic line lies close to or outside of the computational plane (fig. 3), a workable two-strip procedure can be created by eliminating the requirement of equally spaced strips. When a very narrow strip, $\Delta\eta_1 \lessapprox 0.075$, is placed close to the body and a second wide strip is used to complete the shock layer, it is found that solutions can be obtained by using the same integration step size as the one-strip methods. Furthermore, the solution became relatively insensitive to the choice of one initial condition v'_{20} (the value of v_{20} on the stagnation line which satisfies all convergence criteria to the sonic corner). Consequently, the solution procedure behaves like a one-strip MIR if a reasonable specification can be made for v'_{20}. By assuming a quadratic pressure variation across the stagnation line with $\frac{\partial p}{\partial \eta} = 0$ at $\eta = 0$, one can write

$$p_{20} = p_{stag} + (p_s - p_{stag})(\Delta\eta_1)^2 \tag{19}$$

This value of p_{20} can be used to calculate v'_{20} from the limiting form of the governing equations on the stagnation line. The reformulation of this two-strip problem requires another derivation of the governing equations. Now, rather than integrating from $(K - 1)/N$ to K/N in equation (5), it is necessary to substitute the proper values of η at each strip boundary. The only change which results is in the strip constants of equations (12). These strip constants are now expressed as follows:

$$\left.\begin{aligned}
C_1 &= \overline{BPA2}\, r_b + \overline{BB3}\, \delta \cos\theta_b \\
C_2 &= (1 + \delta Q\, \overline{B1})(r_b + \delta\, \overline{B1} \cos\theta_b) \\
C_3 &= -(1 + \delta Q\, \overline{A1})(r_b + \delta\, \overline{A1} \cos\theta_b) \\
C_4 &= \delta\left(\overline{BMA2}\, \frac{dr_b}{ds} - \overline{BB1}\, \delta \sin\theta_b \frac{d\theta_b}{ds}\right) \\
C_5 &= \delta\left(\overline{BMA2}\, \frac{dr_b}{ds} - \overline{BB2}\, \delta \sin\theta_b \frac{d\theta_b}{ds}\right) \\
C_6 &= \delta(\overline{BMA2}\, r_b + \overline{BB1}\, \delta \cos\theta_b) \\
C_7 &= \delta(\overline{BMA2}\, r_b + \overline{BB2}\, \delta \cos\theta_b) \\
C_8 &= -\delta \cos\theta_b(\overline{BMA2} + \overline{BB1}\, \delta Q) \\
C_9 &= -\delta \cos\theta_b(\overline{BMA2} + \overline{BB2}\, \delta Q)
\end{aligned}\right\} \tag{20}$$

where

$$\overline{BB1} = (\overline{B1} + \overline{2A1})\overline{BMA2}/3$$

$$\overline{BB2} = (\overline{2B1} + \overline{A1})\overline{BMA2}/3$$

$$\overline{BB3} = (\overline{B1}^2 + \overline{A1}\ \overline{B1} + \overline{A1}^2)/3$$

$$\overline{BPA2} = (\overline{B1} + \overline{A1})/2$$

$$\overline{BMA2} = (\overline{B1} - \overline{A1})/2$$

$$\overline{A1} = (K - 1)\Delta\eta_1$$

$$\overline{B1} = \Delta\eta_1 + (K - 1)(1 - \Delta\eta_1)$$

The two-strip solution procedure described requires adjustment on only one initial condition and has been used as a tool for assessing the effectiveness of the MIR for use in predicting radiative heating over sonic corner bodies.

RESULTS AND DISCUSSION

Flow field calculations have been made over spherically capped cones and hyperbolic bodies of revolution with the numerical techniques described herein. All the body shapes considered are characterized by having the sonic line of the flow field attached at the aft corner of the body. All the solutions are obtained for hydrogen-helium gas mixtures because of the current interest in exploration of the outer planets by instrumented probes.

A time asymptotic technique (TAT) as developed by Sutton (ref. 7), for inviscid, radiating flow fields has been used as a basis for all the comparisons. The technique, which has been tested against other flow field routines and experimental data, has been found to be an accurate, reliable method which has been used extensively for making radiative heating calculations over planetary probes (ref. 13). The TAT was initially developed for treating smooth bodies without sonic corners, but a program modification allows a special treatment of the governing equations at the aft corner of the body to treat a sonic condition by following the method of Barnwell (refs. 14 and 15). However, the program modification fails when the sonic line of the flow field moves outside of the computational domain of a body-oriented coordinate system. This failure occurs because the backward difference formulas used to obtain the outflow boundary conditions in the TAT are only valid in a supersonic domain. (Barnwell uses polar coordinates at the corner to overcome this problem, but Sutton's program was never modified in this manner.) Consequently, for given free-stream conditions, all comparisons are made where the upper bound on the body angle is restricted so that the sonic line is within the TAT computational domain, and the lower bound on the body angle is restricted so that subsonic flow exists along the body to the aft corner as required by the present method.

Solutions are obtained for the following free-stream conditions:

Case I:

$C_H = 0.74$

$C_{He} = 0.26$

$V_\infty^* = 39.09$ km/s

$\rho_\infty^* = 4.65 \times 10^{-4}$ kg/m^3

$p_\infty^* = 244$ N/m^2

Case II:

$C_H = 0.79$

$C_{He} = 0.21$

$V_\infty^* = 28.19$ km/s

$\rho_\infty^* = 1.06 \times 10^{-3}$ kg/m^3

$p_\infty^* = 0$ N/m^2

Case III:

$C_H = 0.79$

$C_{He} = 0.21$

$V_\infty^* = 31.90$ km/s

$\rho_\infty^* = 7.98 \times 10^{-4}$ kg/m^3

$p_\infty^* = 0$ N/m^2

Case IV:

$C_H = 0.79$

$C_{He} = 0.21$

$V_\infty^* = 39.09$ km/s

$\rho_\infty^* = 3.90 \times 10^{-4}$ kg/m^3

$p_\infty^* = 0$ N/m^2

Case V:

$C_H = 0.20$

$C_{He} = 0.80$

$V_\infty^* = 18.13$ km/s

$\rho_\infty^* = 2.99 \times 10^{-3}$ kg/m^3

$p_\infty^* = 0$ N/m^2

(Free-stream pressures equal to zero are acceptable specifications because the static pressure contribution to the momentum relationships across the shock are extremely small at these velocities.) Execution time for the MIR routine is approximately two to three times faster than that for the TAT for all of the solutions presented herein.

Both MIR and TAT use subroutine RAD/EQUIL to calculate the radiative heating (ref. 9). Cases II to V were run with the same version of RAD/EQUIL (RAD 69). An updated version of subroutine RAD/EQUIL (RAD 73) is incorporated into the TAT for the purpose of calculating Case I. RAD 73 has been streamlined for faster computations and it treats the hydrogen line contribution to the radiation in a more accurate manner. The MIR uses the RAD 69 version for all the cases. The input data deck for RAD 69 is modified to reflect some of the internal changes in the way RAD 73 treats the hydrogen lines. It is seen in figure 7 that both versions of RAD/EQUIL yield radiative heating results which agree closely for a given thermodynamic distribution across the shock layer typical of Case I.

Figure 8 presents adiabatic results for surface pressure and shock displacement distributions corresponding to Case I for a 70° hyperbola with a nose radius to base radius ratio of 0.5 ($R_N^* = 0.223$ m). The MIR prediction of surface pressure is approximately 7 percent less than predictions made by the more exact TAT in the region ahead of the sonic corner. This type of underprediction is typical of a single-strip MIR when applied to sonic corner bodies, as observed by South (ref. 3) and Jones, et al. (ref. 16) in comparisons made with experimental data. Shock standoff distance is also underpredicted in this case, especially near the sonic corner.

The previous case was also computed by including the effect of radiative heat transfer. With radiation transfer, the shock layer experiences radiation cooling due to the radiation that escapes through the shock. The nonadiabatic results are shown in figure 9. Note that there is fair agreement between both methods in the stagnation region for shock standoff distance and surface radiative heating. For this case, the MIR overpredicts the shock standoff distance for about one-half of the forebody when compared with the TAT. Also the nonadiabatic shock standoff distance is considerably less than the corresponding adiabatic value. For example, at the stagnation point, the TAT predicts a 17-percent decrease in δ_{stag} while the MIR predicts only an 8-percent decrease. At the aft corner of the body, the TAT predicts a 9-percent decrease in δ whereas the MIR predicts only a 3-percent decrease. The comparison of

radiative heating predictions closely follows the trend of the shock standoff distance predictions. The largest differences between the two prediction techniques occur along the body near the sonic corner.

The differences in the percent change of δ_{stag} brought about by radiation transfer point out the insensitivity of the MIR relative to that of the TAT. This insensitivity is a consequence of the linear approximations in equations (4) of properties across the shock layer for a one-strip MIR. Profiles of flow field variables as predicted by the two techniques are compared in figures 9(b) and 9(c). Note the large gradient in ρ and h predicted by the TAT near the body. On the stagnation line, there is good agreement between ρ and h as predicted by both methods over most of the shock layer. However, the radiative cooling near the wall causes the surface values of ρ and h to differ by 19 percent and 42 percent, respectively. (Percent difference is defined by $\frac{\text{MIR prediction - TAT prediction}}{\text{TAT prediction}} \times 100.$)

Pressure predictions agree within 3 percent on the stagnation line. A quadratic variation of pressure across the shock layer was also tried in several cases. Although MIR pressure profiles with a quadratic variation agreed more closely with the TAT pressure profiles in the stagnation region, there was little effect on the overall flow field predictions.

Further downstream at a body station $s = 1.4$, density and enthalpy profiles (fig. 9(c)) follow much the same pattern as in the stagnation region. There is a larger percentage difference between the comparisons for density and pressure than occurred at the axis of symmetry. The TAT also predicts a larger mass flow rate near the body as compared with the MIR solution (fig. 9(c)) which is locked into a linear variation across the shock layer according to the assumptions made in equations (4).

When flow field solutions are obtained over less blunt bodies, the MIR predictions show larger differences as compared with predictions by TAT. Figures 10 to 12 show shock standoff distance and radiative heating distributions calculated by both the MIR and the TAT for Cases II, III, and IV over a spherically capped cone ($\theta_c = 60^o$, $R_N^*/r_B = 0.5$, and $R_N^* = 0.223$ m). These conditions correspond to trajectory points for an entry into a Jovian atmosphere as reported in reference 13.

The comparisons between the two methods are poor. Shock standoff distance is accurately predicted in the stagnation region, but it is significantly overpredicted by the MIR along the cone in every case. The radiative heating levels on the cone are also too high. Some insight into these large discrepancies can be gained by looking at the details of the flow profiles for one of these cases.

Density, enthalpy, and pressure profiles across the shock layer at two body locations for Case IV are presented in figure 13. The comparisons here between the MIR and TAT are similar to those presented in figure 9. There is a large difference between the two methods in the ρu profile across the shock layer. Because the TAT calculates a larger mass flow rate than the MIR, it

follows that the TAT will yield a smaller shock standoff distance than the MIR at this location. In general, the shock layer thicknesses along with the pressure and temperature levels are critical parameters for determining radiative heating levels on planetary probes (ref. 13). The large enthalpy levels near the wall and the large shock standoff distances predicted with the MIR combine to cause large radiative heating levels compared with TAT results.

Results of calculations for Case V (spherically capped cone, $\theta_c = 62^\circ$, $R_N^*/r_B = 0.5$, and $R_N^* = 0.223$ m) are presented in figure 14. This case is one for which a two-strip solution could be obtained, as described in the previous section. (Free-stream conditions for Case V are those for an entry into Uranus as reported in ref. 13.)

Pressure and temperature distributions are presented in figures 14(a) and 14(b). The two-strip solution improves the MIR pressure prediction as compared with the TAT, except near the sphere cone junction where a bump occurs in the pressure distribution. This bump increased in height as the inner strip height decreased. The bump is caused by the discontinuity in body curvature at the sphere cone junction. No such irregularities were obtained on any two-strip solutions of continuous curvature bodies. Because the irregularity was confined to a small area of the flow field, no special differencing or smoothing procedures were incorporated to try to eliminate this problem.

The TAT results for temperature variation are shown at nondimensional distance of $\eta = 0$ (body) and $\eta = 0.07$. The one-strip MIR agrees closely with the TAT prediction at $\eta = 0.07$. However, there is a 1000-K temperature difference between the TAT results at $\eta = 0$ and $\eta = 0.07$. This difference is indicative of the large gradients in enthalpy profiles near the wall which have been observed in all the nonadiabatic results. The two-strip MIR agrees more closely with the TAT result for temperature at $\eta = 0$ than with the one-strip method. However, even the two-strip method is unable to predict the same large decrease in temperature near the wall as the TAT. (See figs. 14(b), 14(e), and 14(f).)

Shock standoff and surface radiative heating distributions are presented in figures 14(c) and 14(d), respectively. There is good agreement in the stagnation region among all three methods for shock standoff distance. The two-strip MIR and the TAT results agree closely over the entire body. The two-strip MIR heating distribution is in good agreement with the TAT results over the entire body. The one-strip MIR radiative heating distribution shows fair agreement with the TAT in the stagnation region, but it falls below the TAT results over the cone.

The improved comparisons of the two-strip MIR calculations with the TAT calculations can be explained by examining the shock layer property profiles shown in figures 14(e) and 14(f). There is very little difference between the one- and two-strip solutions for the density, enthalpy, pressure, and velocity profiles on the stagnation line except near the body. Near the body, the enthalpy profile calculated by the two-strip MIR is much closer to the TAT result than the profile calculated by the one-strip MIR. However, it is clear that even with a two-strip solution, the enthalpy gradient is not nearly as great as that calculated by the TAT. Density, enthalpy, pressure, and mass flux

profiles calculated by using a two-strip MIR are still in good agreement with TAT profiles at a body location $s = 1.5$ (fig. 14(f)). The small bump which occurs in the two-strip MIR density profile near the wall is a consequence of the linear approximations made on ρu and ρu^2 across the narrow strip.

$$\left(\text{Note that } \rho(\eta) = [\rho u(\eta)]^2 / [\rho u^2(\eta)].\right)$$

Comparisons between the one- and two-strip MIR are presented in figure 15 for Case V with various cone angles. The relative difference between the one- and two-strip radiative heating rate values becomes smaller as the cone angle increases.

The two-strip MIR can resolve the enthalpy and density gradients near the wall better than the one-strip MIR. The two-strip MIR also calculates a more accurate pressure distribution around the flank of sonic corner bodies. However, the two-strip MIR has an extremely limited range of applicability. The method can only be used when the sonic line lies near the computational boundary (fig. 4). In the one comparison case that was available with the TAT, the two-strip MIR calculated radiative heating levels that were within 10 percent of the TAT values over most of the body. No other cases with entry conditions significantly different from the one presented were found that could be calculated by using both the TAT and the two-strip MIR.

One serious drawback of the two-strip method is that the procedure is not truly closed. The ability of the two-strip method to converge depends on the accuracy of the assumption that the sonic line lies very close to or outside of the border of the computational domain at the aft corner of the body. Usually, if that assumption is incorrect, the program will fail to converge to any solution with the two-strip method. However, some cases have been found where the two-strip method converged to a physically unrealistic solution. Also, the two-strip method is not always superior to the one-strip method. For example, there is little difference in the radiative heating results between the one- and two-strip methods for large cone angles (fig. 15). Consequently, the range of conditions over which the two-strip method can offer any significant improvement over the one-strip method is small.

CONCLUDING REMARKS

The one-strip method of integral relations is unreliable in making radiative heating calculations over planetary probes with sonic corners. The method yields surface pressures which are too low near the sonic corner and is unable to resolve enthalpy and density gradients near the wall. As the solution is marched downstream from the stagnation line, these errors combine to produce gross distortions of the radiative heating levels to the surface.

A modification of a two-strip method of integral relations, as described herein, does a better job of resolving the enthalpy and density gradients near the wall than the one-strip method; however, the gradients predicted by the two-strip method are still not quite as severe as those predicted by the time asymptotic technique. The two-strip method does not distort the pressure dis-

tribution around the body as severely as the one-strip method. In the one detailed comparison case with the time asymptotic technique, the two-strip method of integral relations accurately predicted the radiative heating levels over the entire body.

Very little difference was observed in the radiative heating distributions between the one- and two-strip methods for very large cone angles ($\theta_c > 75^o$). Thus, for the very blunt bodies, there seems to be little advantage in going to the two-strip method. There is also the possibility that the two-strip method can converge to a physically unrealistic solution because the procedure is not truly closed.

Consequently, the one-strip method of integral relations cannot be relied on to obtain accurate estimates of radiative heating over planetary probe vehicles for the conditions described herein. In some instances, a two-strip method can be used to improve these estimates. However, the small range over which the two-strip method can offer significant improvement over the one-strip method makes it unrealistic to pursue further development of this technique.

Langley Research Center
National Aeronautics and Space Administration
Hampton, VA 23665
December 21, 1977

APPENDIX

LOCALLY VALID RELATIONS FOR EQUATION OF STATE AND SPEED OF SOUND

Subroutine RAD/EQUIL (ref. 9) is used to obtain density, the mole fraction of the considered species, the ratio of specific heats, and temperature as a function of pressure and static enthalpy for arbitrary gas mixtures. An equation of state for a real gas in chemical equilibrium must be coupled with the other governing equations to obtain a flow field solution. A successive substitution algorithm is time consuming, and in the region near the sonic line singularity, the successive substitution can diverge. It is desirable to derive a local equation of state at each point in the flow field which is valid over the small range of anticipated pressures and enthalpies at that point. This analytic equation of state is then coupled with the other governing equations and the entire system of equations is solved by using the quadratically convergent Newton-Raphson technique. It is assumed that a locally valid equation of state can be written as

$$p = A\rho^B h^C \tag{A1}$$

Choose p_a, p_b, and p_c equal to three values of pressure within the anticipated pressure range. Choose h_a, h_b, and h_c equal to three values of enthalpy within the anticipated enthalpy range. (The anticipated pressure range near the axis of symmetry is bounded by the stagnation pressure and the pressure behind the shock which can be obtained directly from RAD/EQUIL. The anticipated enthalpy range near the axis of symmetry is bounded by the stagnation enthalpy and static enthalpy behind the shock. Anticipated ranges of pressure and enthalpy at subsequent computational points are extrapolated from converged values of pressure and enthalpy upstream of the points.)

Let

$$\rho_a = \rho(p_a, h_a)$$

$$\rho_b = \rho(p_b, h_b)$$

$$\rho_c = \rho(p_c, h_c)$$

where $\rho(p,h)$ is obtained from subroutine RAD/EQUIL. If equation (A1) is to be valid, the following equations must be true:

$$\left.\begin{aligned} p_a &= A\rho_a{}^B h_a{}^C \\ p_b &= A\rho_b{}^B h_b{}^C \\ p_c &= A\rho_c{}^B h_c{}^C \end{aligned}\right\} \tag{A2}$$

APPENDIX

Taking the logarithm of both sides of equations (A2) and solving for A, B, and C yields

$$C = \frac{\left[\log_e (\rho_a/\rho_c) \log_e (p_a/p_b) - \log_e (\rho_a/\rho_b) \log_e (p_a/p_c)\right]}{\left[\log_e (\rho_a/\rho_c) \log_e (h_a/h_b) - \log_e (\rho_a/\rho_b) \log_e (h_a/h_c)\right]} \tag{A3}$$

$$B = \frac{\left[\log_e (h_a/h_c) \log_e (p_a/p_b) - \log_e (h_a/h_b) \log_e (p_a/p_c)\right]}{\left[\log_e (h_a/h_c) \log_e (\rho_a/\rho_b) - \log_e (h_a/h_b) \log_e (\rho_a/\rho_c)\right]} \tag{A4}$$

$$A = p_a \rho_a^{-B} h_a^{-C} \tag{A5}$$

Values for A, B, and C are calculated in this manner at the boundary of every strip and at every integration step around the body. These values are updated at every pass around the body. (Because the pressure and enthalpy levels in the stagnation region do not substantially change during the last few iterations, it should be possible to save values of A, B, and C, and thus save additional calls to RAD/EQUIL. However, the present program was never optimized in this manner.)

A comparison of results for density obtained by using a local equation of state and a direct use of RAD/EQUIL are presented in table I.

It is necessary in this analysis to be able to locate the sonic line in the flow field. A speed of sound must therefore be calculated at every computational point in the flow field. The speed of sound is defined as

$$a^* = \sqrt{\gamma R_g^* T^*}$$

However, γ, R_g^*, and T^* are functions of pressure and enthalpy for arbitrary gas mixtures. Since a local equation of state must be determined at every computational point, it is convenient to determine a local equation for the speed of sound simultaneously, and thus eliminate an additional call to RAD/EQUIL.

It is again assumed that a local equation for the speed of sound can be written as

$$a = D \rho^E p^F$$

By following the development in the previous section, it is found that

$$F = \frac{\left[\log_e (\rho_a/\rho_c) \log_e (a_a/a_b) - \log_e (\rho_a/\rho_b) \log_e (a_a/a_c)\right]}{\left[\log_e (\rho_a/\rho_c) \log_e (p_a/p_b) - \log_e (\rho_a/\rho_b) \log_e (p_a/p_c)\right]} \tag{A6}$$

$$E = \frac{\left[\log_e (p_a/p_c) \log_e (a_a/a_b) - \log_e (p_a/p_b) \log_e (a_a/a_c)\right]}{\left[\log_e (p_a/p_c) \log_e (\rho_a/\rho_b) - \log_e (p_a/p_b) \log_e (\rho_a/\rho_c)\right]} \tag{A7}$$

$$D = a_a \rho_a^{-E} p_a^{-F} \tag{A8}$$

where

$$a_a = a(p_a, h_a)$$

$$a_b = a(p_b, h_b)$$

$$a_c = a(p_c, h_c)$$

and p's, ρ's, and h's with subscripts a, b, and c are defined in the previous section. A comparison of results for speed of sound obtained by use of a local equation for the speed of sound and a direct use of RAD/EQUIL are presented in table I.

REFERENCES

1. Suttles, John T.: A Method of Integral Relations Solution for Radiating, Nonadiabatic, Inviscid Flow Over a Blunt Body. NASA TN D-5480, 1969.

2. Edquist, C. T.: Aeroheating of Sphere Cones and Spherical Segment Probes During Venus Entry. Tech. Note P73-203434-061, Rev. A, Martin Marietta Aerospace, Feb. 1973.

3. South, Jerry C., Jr.: Calculation of Axisymmetric Supersonic Flow Past Blunt Bodies With Sonic Corners, Including a Program Description and Listing. NASA TN D-4563, 1968.

4. Rao, P. P.: Supersonic Flow Around Concave and Convex Blunt Bodies. Trans. ASME, Ser. I: J. Fluids Eng., vol. 95, no. 1, Mar. 1973, pp. 159-161.

5. Belotserkovskiy, O. M., ed.: Numerical Methods for Solving Problems of Mechanics of Continuous Media. NASA TT F-667, 1972.

6. Garrett, L. Bernard; Suttles, John T.; and Perkins, John N. (appendix C by G. Louis Smith and L. Bernard Garrett): A Modified Method of Integral Relations Approach to the Blunt-Body Equilibrium Air Flow Field, Including Comparisons With Inverse Solutions. NASA TN D-5434, 1969.

7. Sutton, Kenneth: Characteristics of Coupled Nongray Radiating Gas Flows With Ablation Product Effects About Blunt Bodies During Planetary Entries. Ph. D. Thesis, North Carolina State Univ., 1973.

8. Sutton, Kenneth; Jones, Jim J.; and Powell, Richard W.: Effect of Probe Configuration on Radiative Heating During Jovian Entry. AIAA Paper No. 76-471, July 1976.

9. Nicolet, W. E.: User's Manual for RAD/EQUIL/1973, a General Purpose Radiation Transport Program. NASA CR-132470, 1973.

10. Miller, Charles G., III: Shock Shapes on Blunt Bodies in Hypersonic-Hypervelocity Helium, Air, and CO_2 Flows, and Calibration Results in Langley 6-Inch Expansion Tube. NASA TN D-7800, 1975.

11. Inouye, Mamoru; Marvin, Joseph G.; and Sinclair, A. Richard: Comparison of Experimental and Theoretical Shock Shapes and Pressure Distributions on Flat-Faced Cylinders at Mach 10.5. NASA TN D-4397, 1968.

12. Holt, Maurice; and Hoffman, Gilbert H.: Calculation of Hypersonic Flow Past Spheres and Ellipsoids. [Preprint] 61-209-1903, American Rocket Soc., June 1961.

13. Sutton, Kenneth: Radiative Heating About Outer Planet Entry Probes. AIAA Paper 75-183, Jan. 1975.

14. Barnwell, Richard W.: Time-Dependent Numerical Method for Treating Complicated Blunt-Body Flow Fields. Analytical Methods in Aircraft Aerodynamics, NASA SP-228, 1970, pp. 177-195.

15. Barnwell, Richard W.: Three-Dimensional Flow Around Blunt Bodies With Sharp Shoulders. AIAA Paper No. 71-56, Jan. 1971.

16. Jones, Robert A; and Hunt, James L.: Measured Pressure Distributions on Large-Angle Cones in Hypersonic Flows of Tetrafluoromethane, Air, and Helium. NASA TN D-7429, 1973.

TABLE I.- COMPARISON OF APPROXIMATE RESULTS CALCULATED BY LOCALLY VALID RELATIONS WITH EXACT RESULTS CALCULATED BY RAD/EQUIL

s	η	Density			Speed of sound		
		Approximate	Exact	Percent difference	Approximate	Exact	Percent difference
Adiabatic							
0	0	10.863889	10.863889	0.00000000	0.32746270	0.32746270	0.00000000
	1	10.413217	10.415360	.02057538	.32580473	.32577076	.01042760
.5	0	10.498678	10.498678	.00000000	.32619309	.32619307	.00000610
	1	10.371731	10.371735	.00003857	.32341920	.32341908	.00003710
1.0	0	10.151106	10.151106	.00000000	.32488561	.32488561	.00000000
	1	10.294323	10.294323	.00000000	.31950323	.31950322	.00000310
1.5	0	9.669698	9.669696	.00002070	.32299906	.32299910	.00001238
	1	10.185146	10.185141	.00004910	.31421897	.31421911	.00004455
2.0	0	8.200939	8.200835	.00126820	.31672379	.31672656	.00087457
	1	9.941612	9.941542	.00070410	.30319808	.30320109	.00099274
Nonadiabatic							
0	0	12.977966	12.977966	0.00000000	0.29983841	0.29983841	0.00000000
	1	10.413217	10.415360	.02057538	.32580473	.32577077	.01042450
.5	0	13.212973	13.212912	.00046170	.29161431	.29161350	.00027780
	1	10.369277	10.369281	.00003858	.32329269	.32329257	.00003710
1.0	0	13.223761	13.223746	.00011340	.28612646	.28612637	.00003150
	1	10.293324	10.293324	.00000000	.31945370	.31945369	.00000310
1.5	0	12.802525	12.802514	.00008590	.28288869	.28288868	.00000350
	1	10.187402	10.187397	.00004910	.31432563	.31432578	.00004772
2.0	0	10.716830	10.716787	.00040120	.27932643	.27932757	.00040812
	1	9.941761	9.941681	.00080470	.30320371	.30320713	.00112794

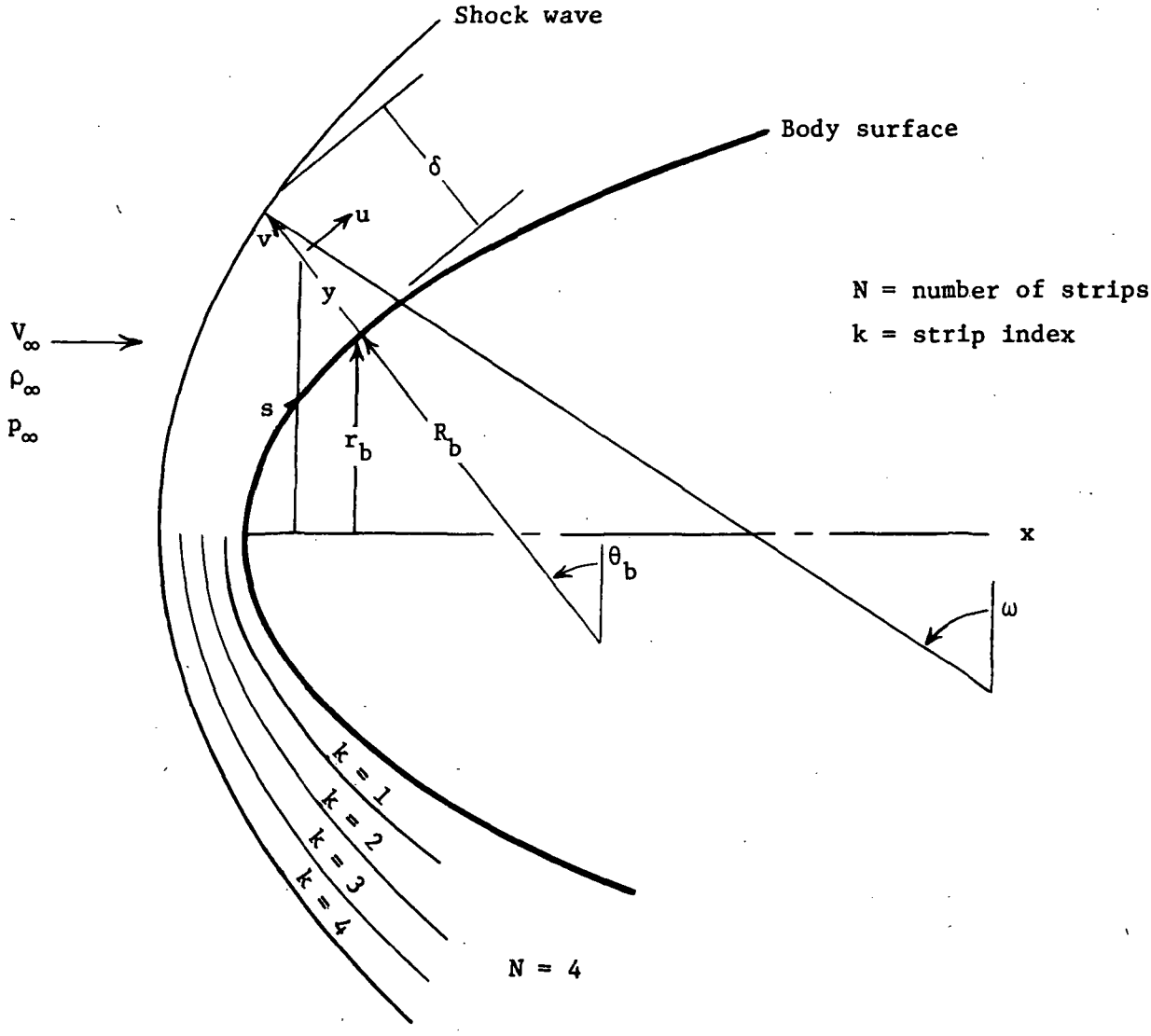

Figure 1.- Coordinate system and strip indexing system.

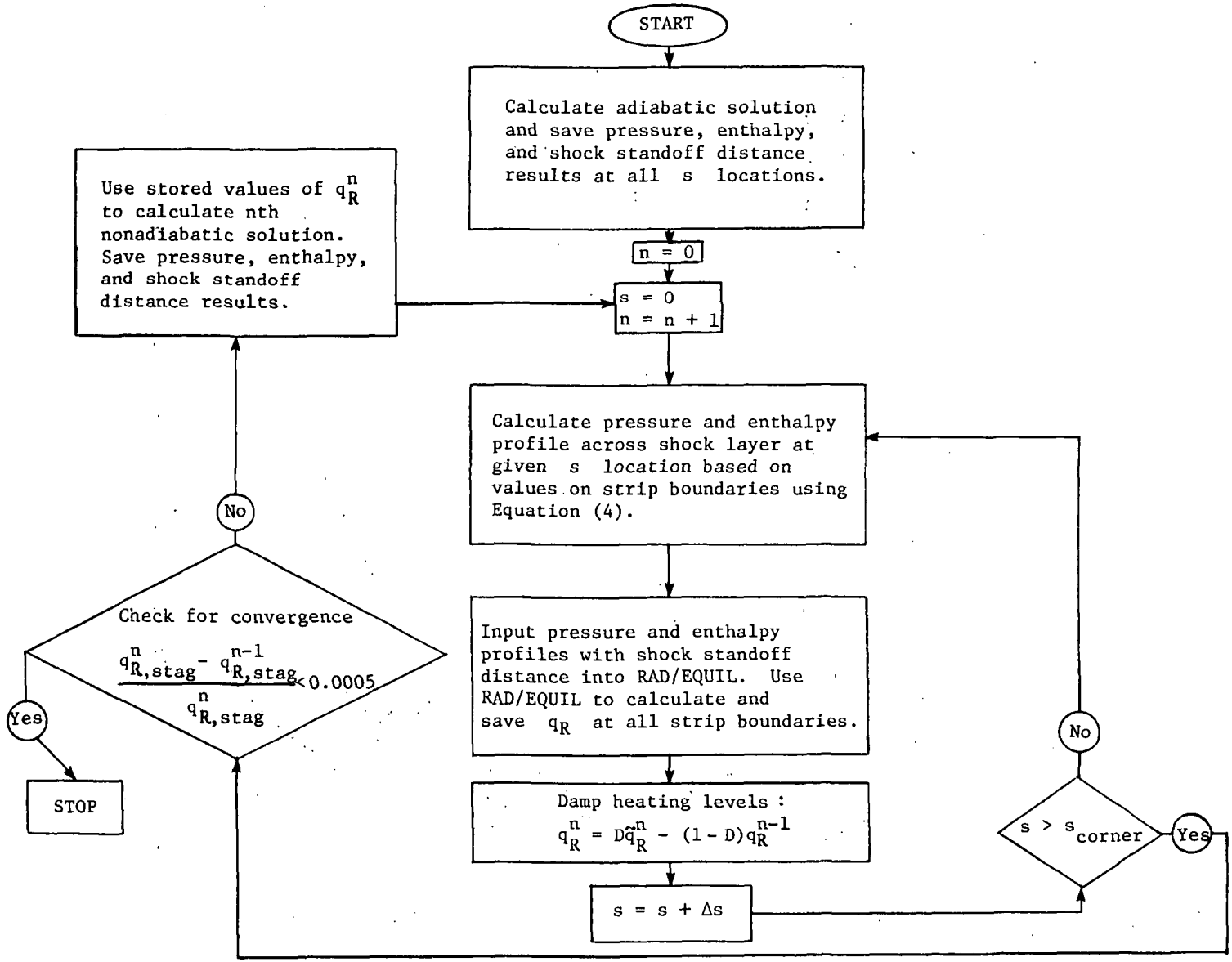

Figure 2.- Flow chart of radiative heating coupling procedure.

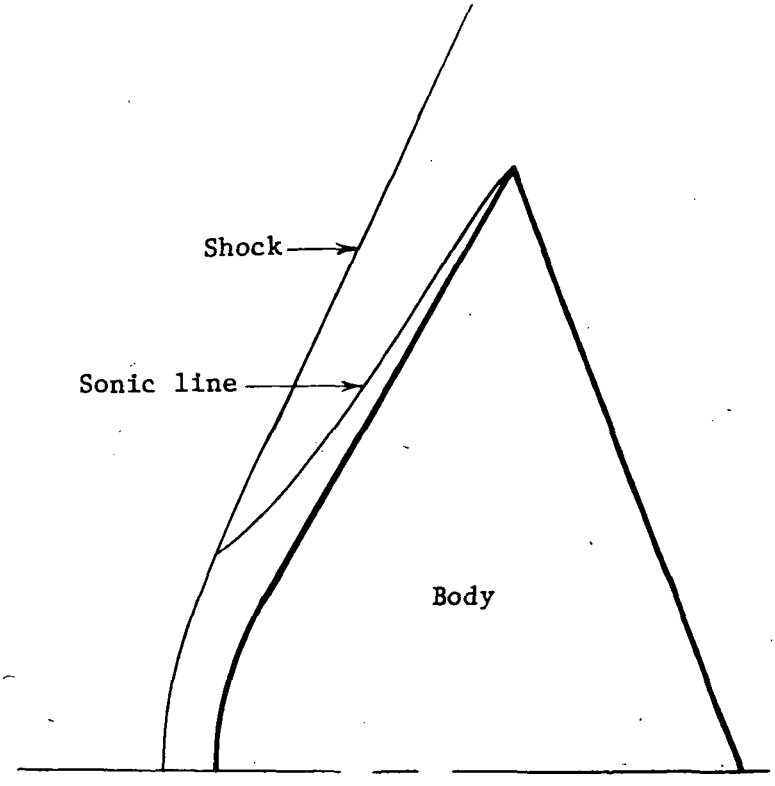

Figure 3.- Sonic line located in computational plane.

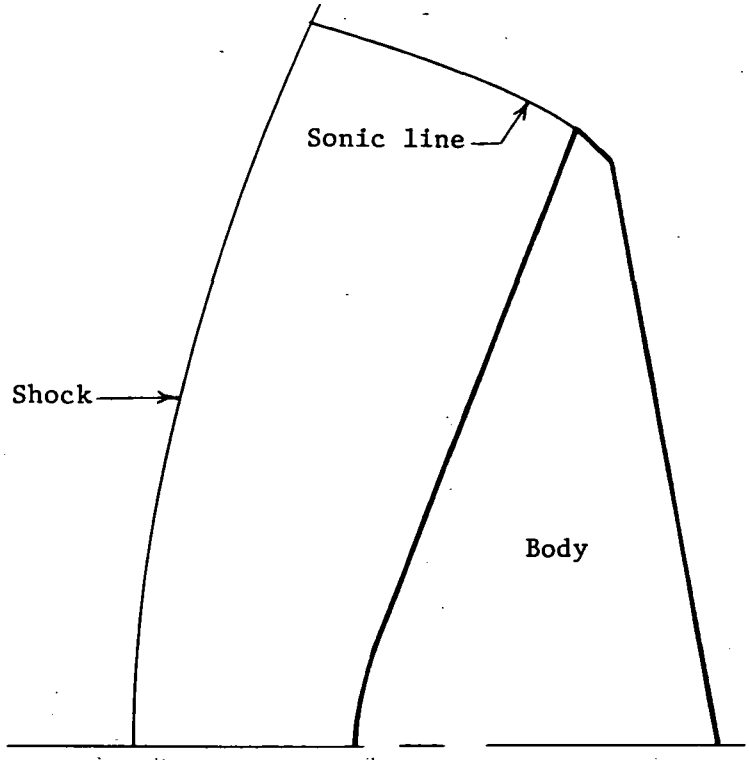

Figure 4.- Sonic line located at boundary of computational plane.

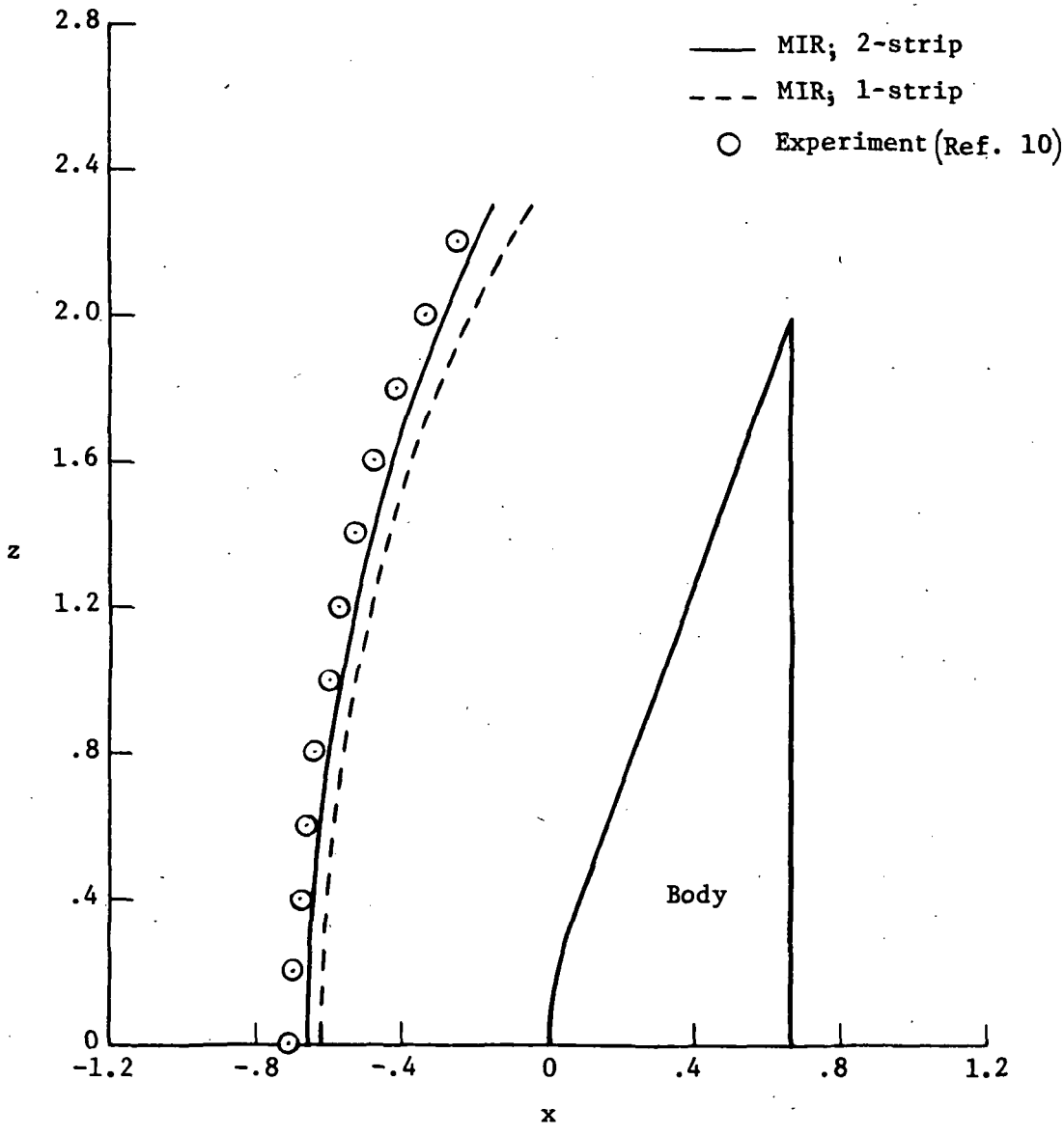

Figure 5.- Comparison of one- and two-strip MIR results for shock shape over 70° spherically capped cone with $R_N/r_B = 0.5$, $M_\infty = 6.02$, and $\gamma = 1.67$.

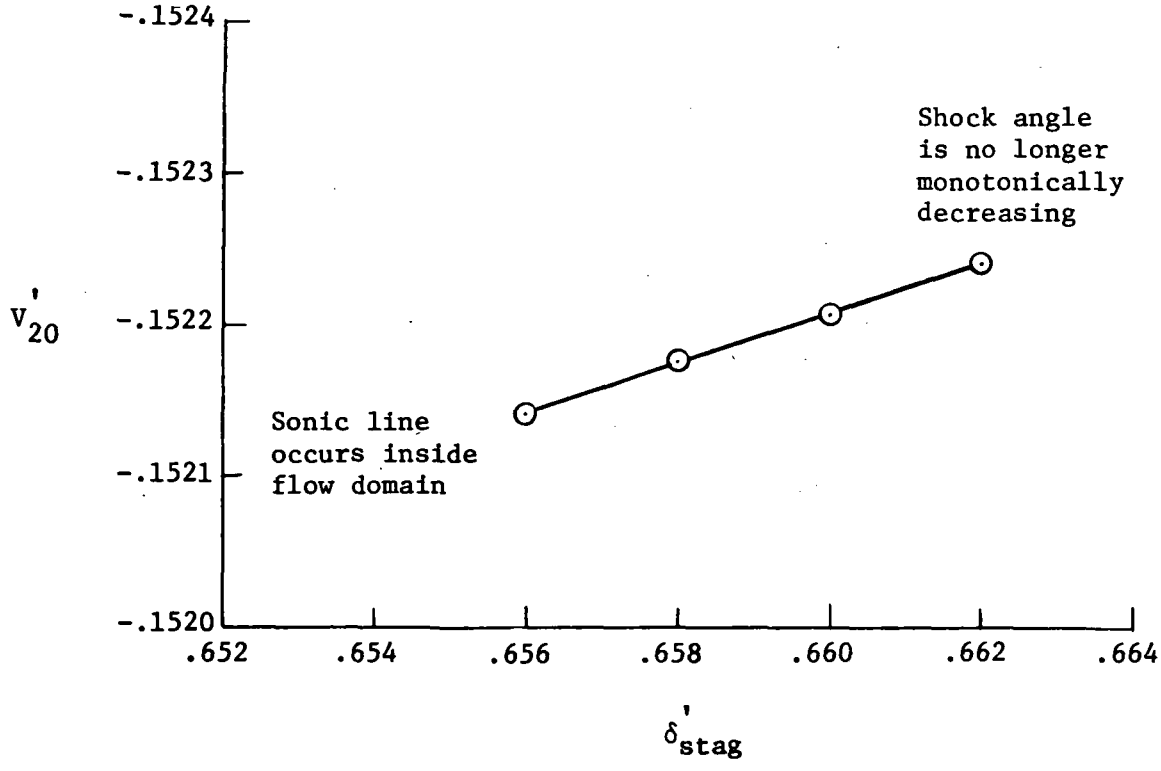

Figure 6.- Initial conditions yielding sonic velocity on corner of body for two-strip solution with $M_\infty = 6.02$, $\gamma = 1.67$, $R_N/r_B = 0.5$, and $\theta_c = 70^\circ$.

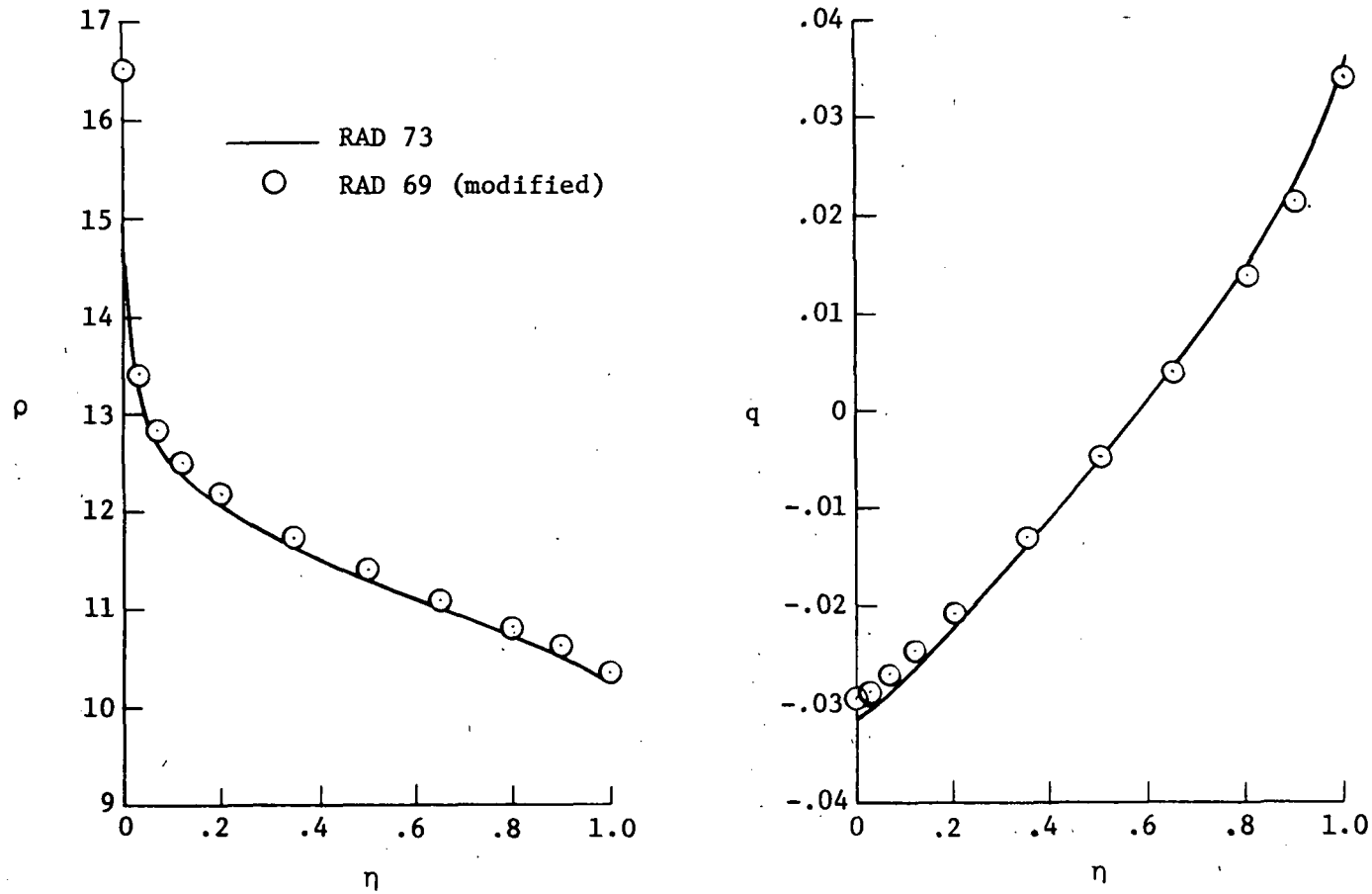

(a) Density profiles.

(b) Radiative flux profiles.

Figure 7.- Comparison of shock layer results using the RAD 73 and the modified RAD 69 radiation subroutines for identical pressure and enthalpy profile inputs.

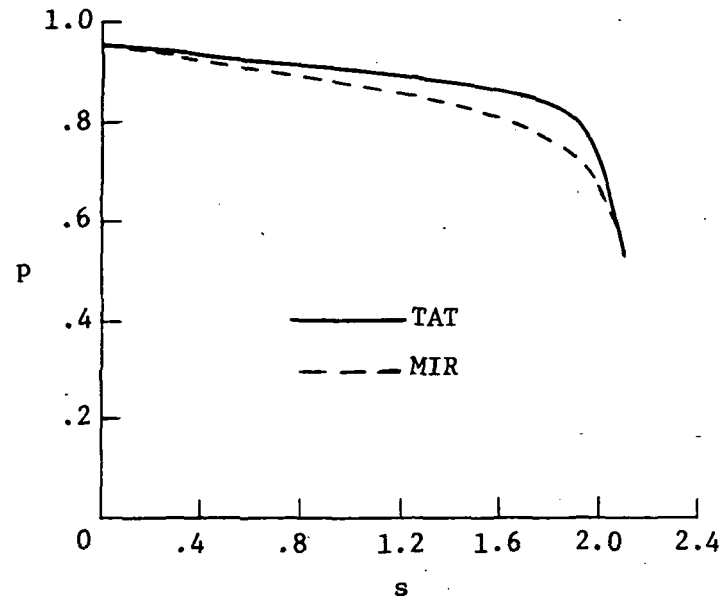

(a) Surface pressure distributions.

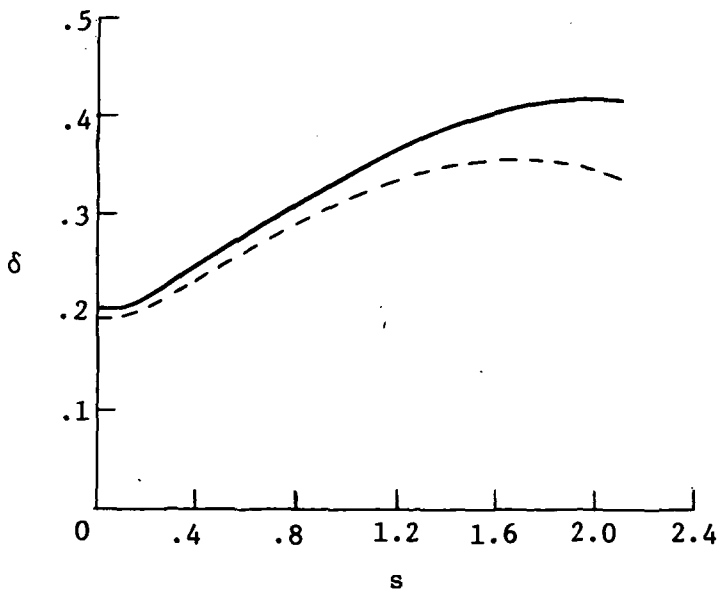

(b) Shock standoff distributions.

Figure 8.- Comparison of MIR calculations with TAT results. Case I; adiabatic.

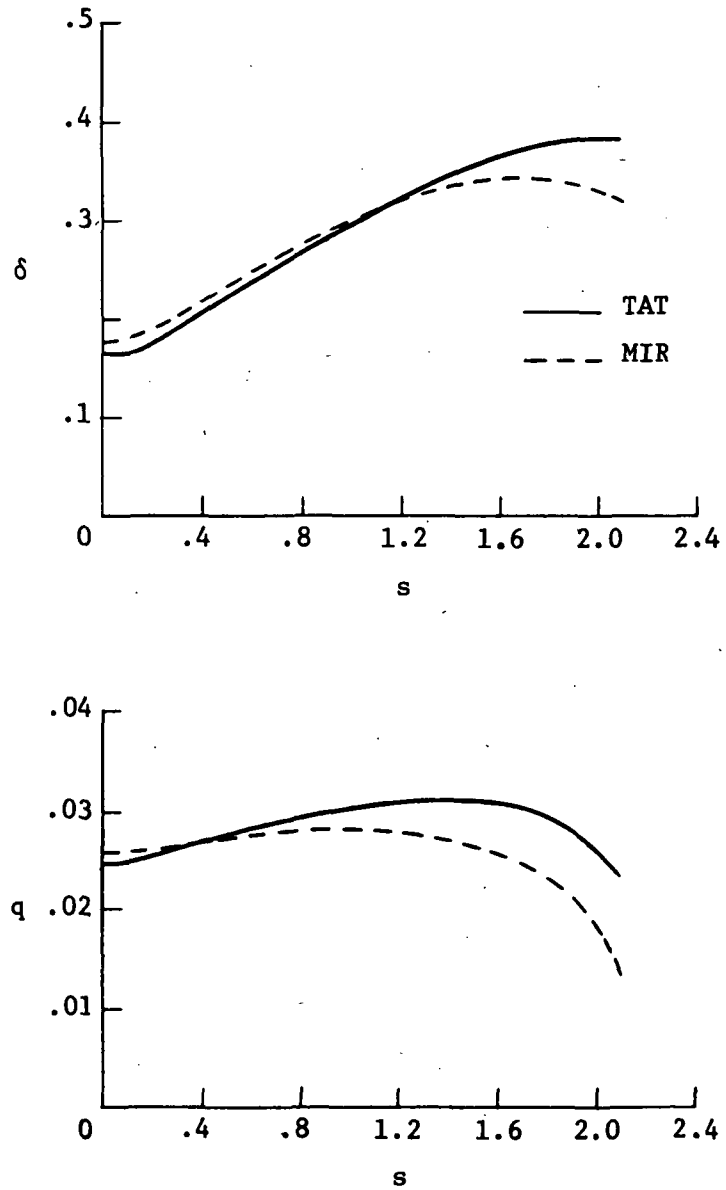

(a) Shock standoff and heat-transfer distributions.

Figure 9.- Comparison of nonadiabatic results for Case I. 70° hyperbola; R_N/r_B = 0.5; and R_N^* = 0.223 m.

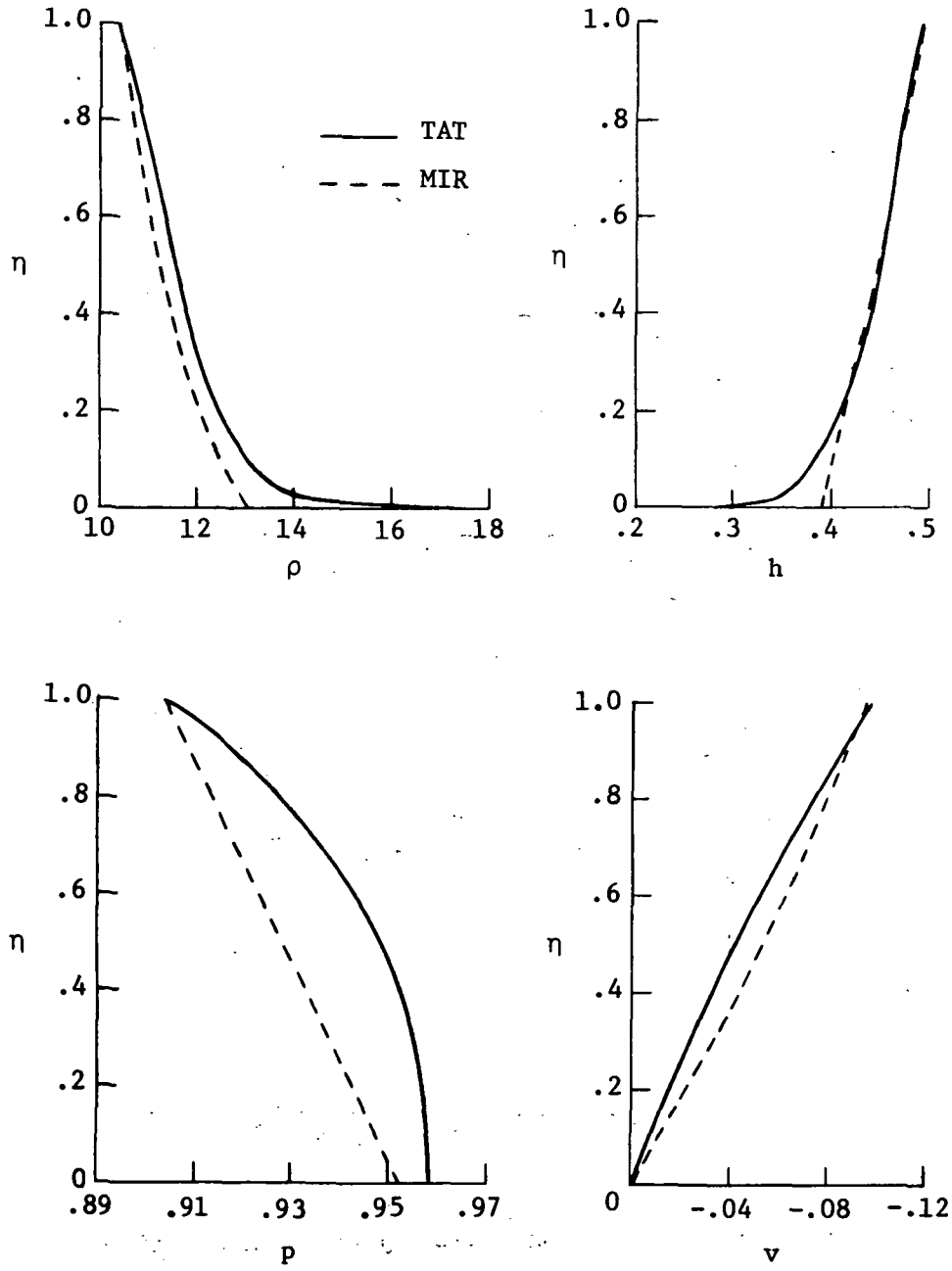

(b) Stagnation line profile properties. s = 0.

Figure 9.- Continued.

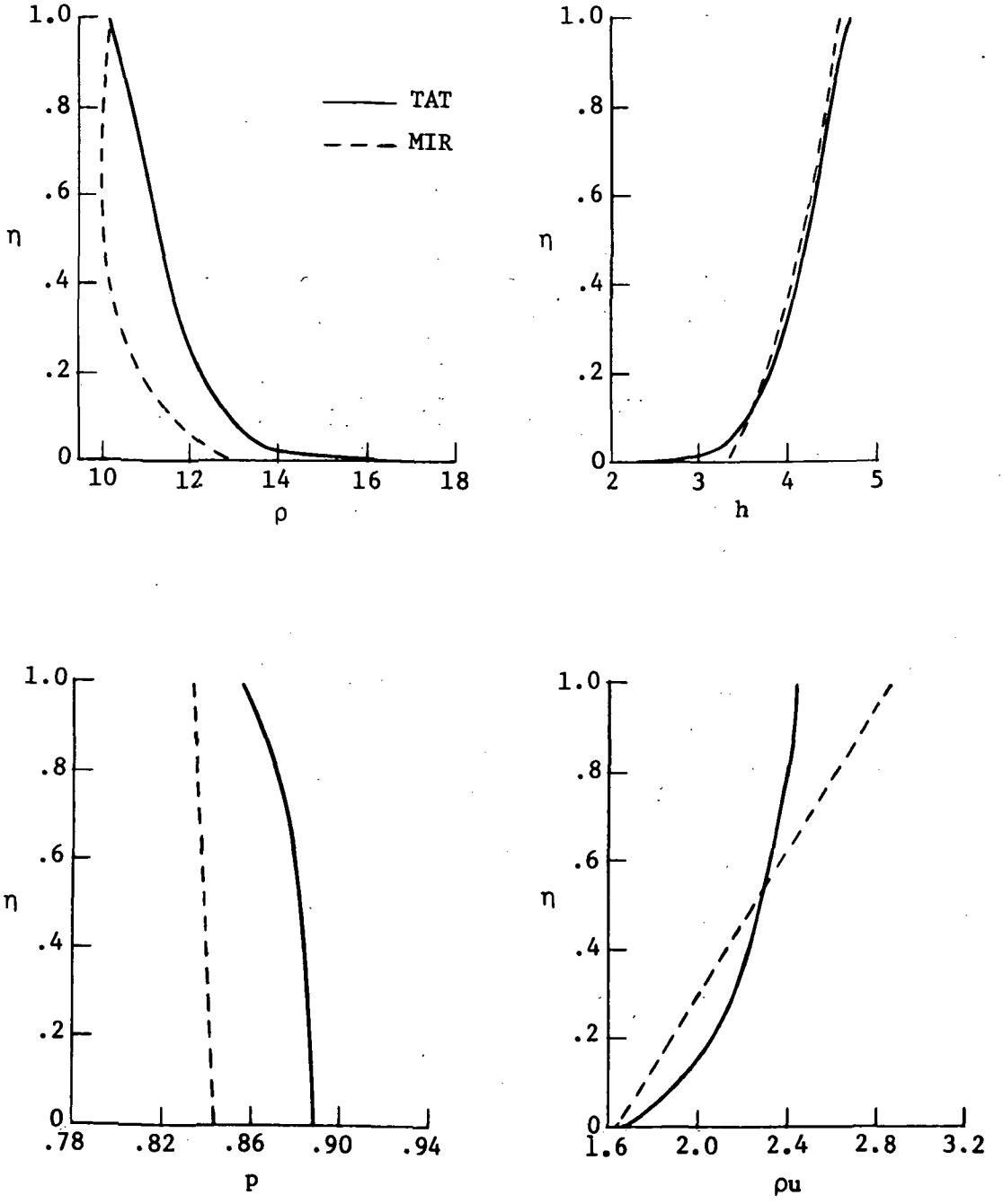

(c) Shock layer profile properties. s = 1.4.

Figure 9.- Concluded.

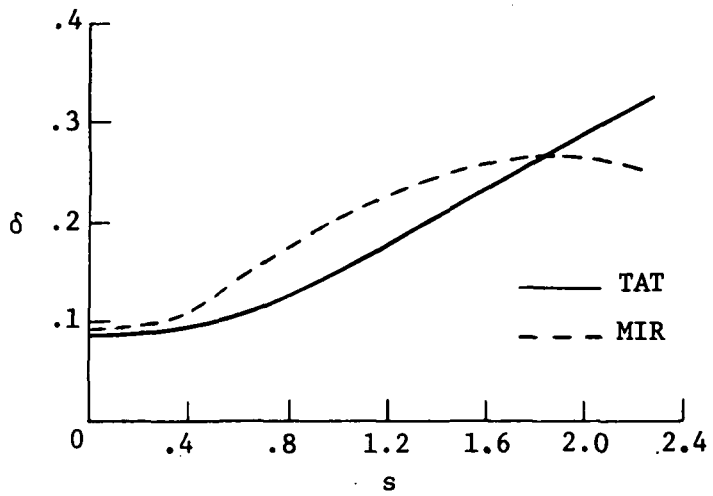

(a) Shock standoff distributions.

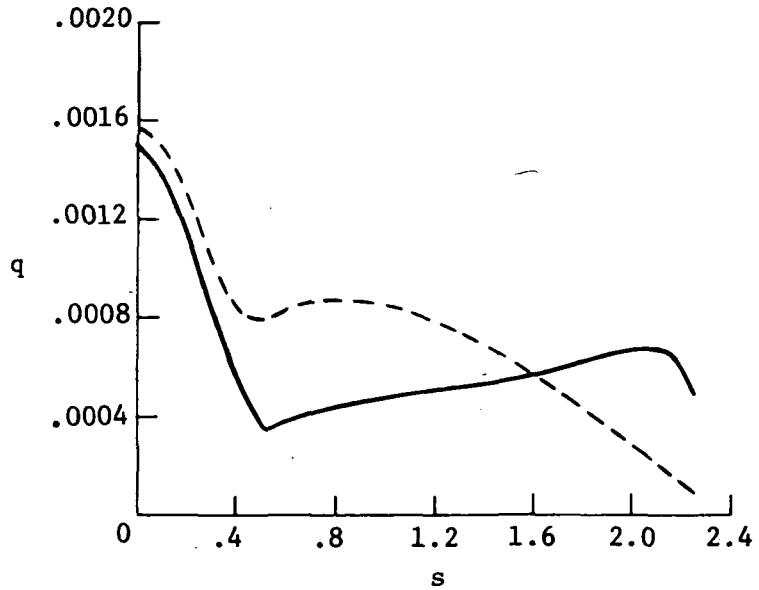

(b) Radiative heat-transfer distributions.

Figure 10.- Comparison of nonadiabatic results for Case II. $\theta_c = 60°$; $R_N/r_B = 0.5$; and $R_N^* = 0.223$ m.

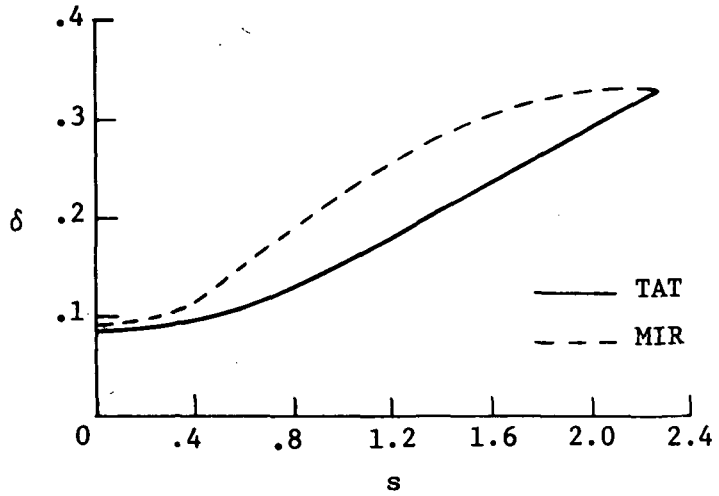

(a) Shock standoff distributions.

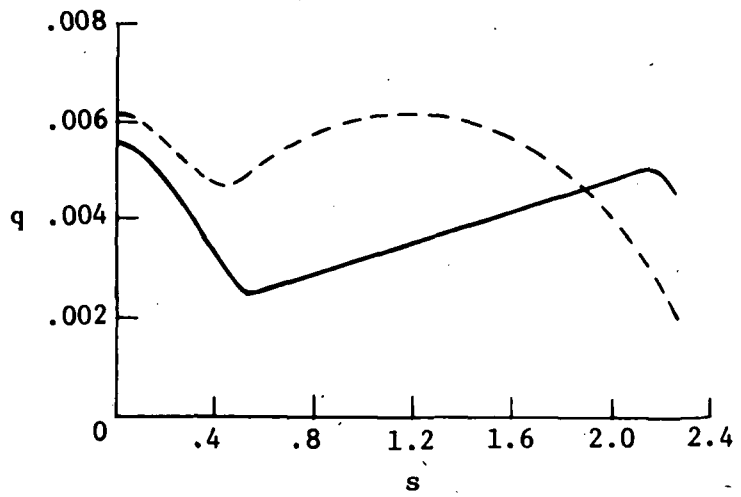

(b) Radiative heat-transfer distributions.

Figure 11.- Comparison of nonadiabatic results for Case III. $\theta_c = 60^\circ$; $R_N/r_B = 0.5$; and $R_N^* = 0.223$ m.

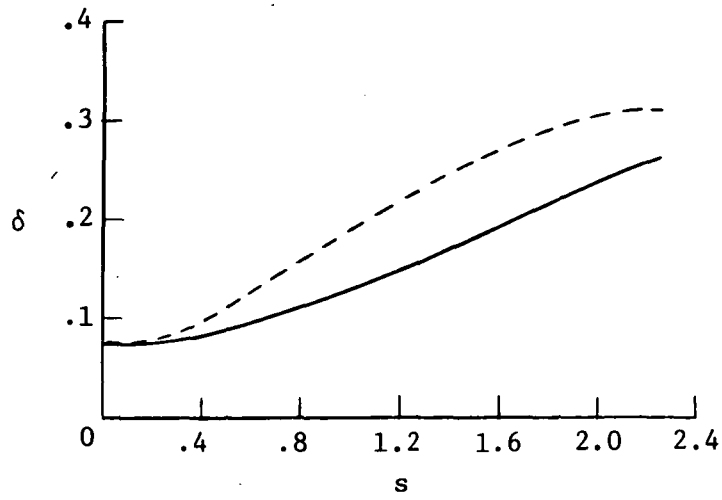

(a) Shock standoff distributions.

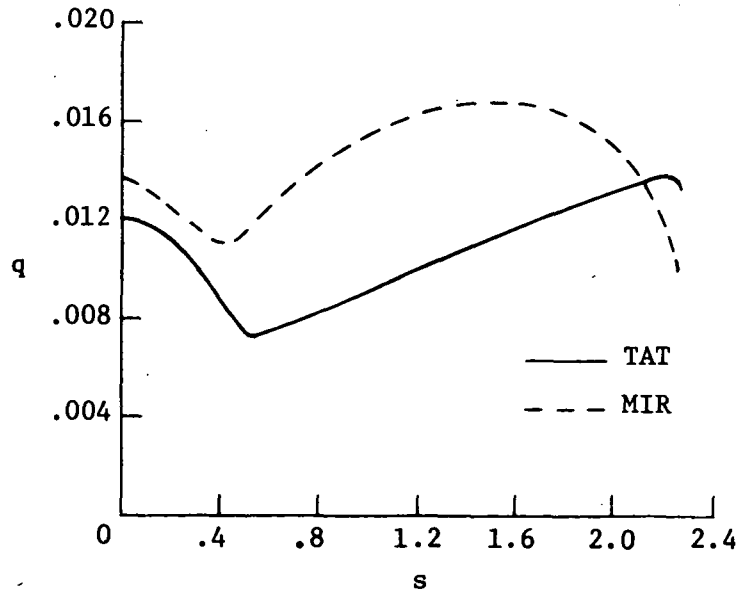

(b) Radiative heat-transfer distributions.

Figure 12.- Comparison of nonadiabatic results for Case IV. $\theta_c = 60°$; $R_N/r_B = 0.5$; and $R_N^* = 0.223$ m.

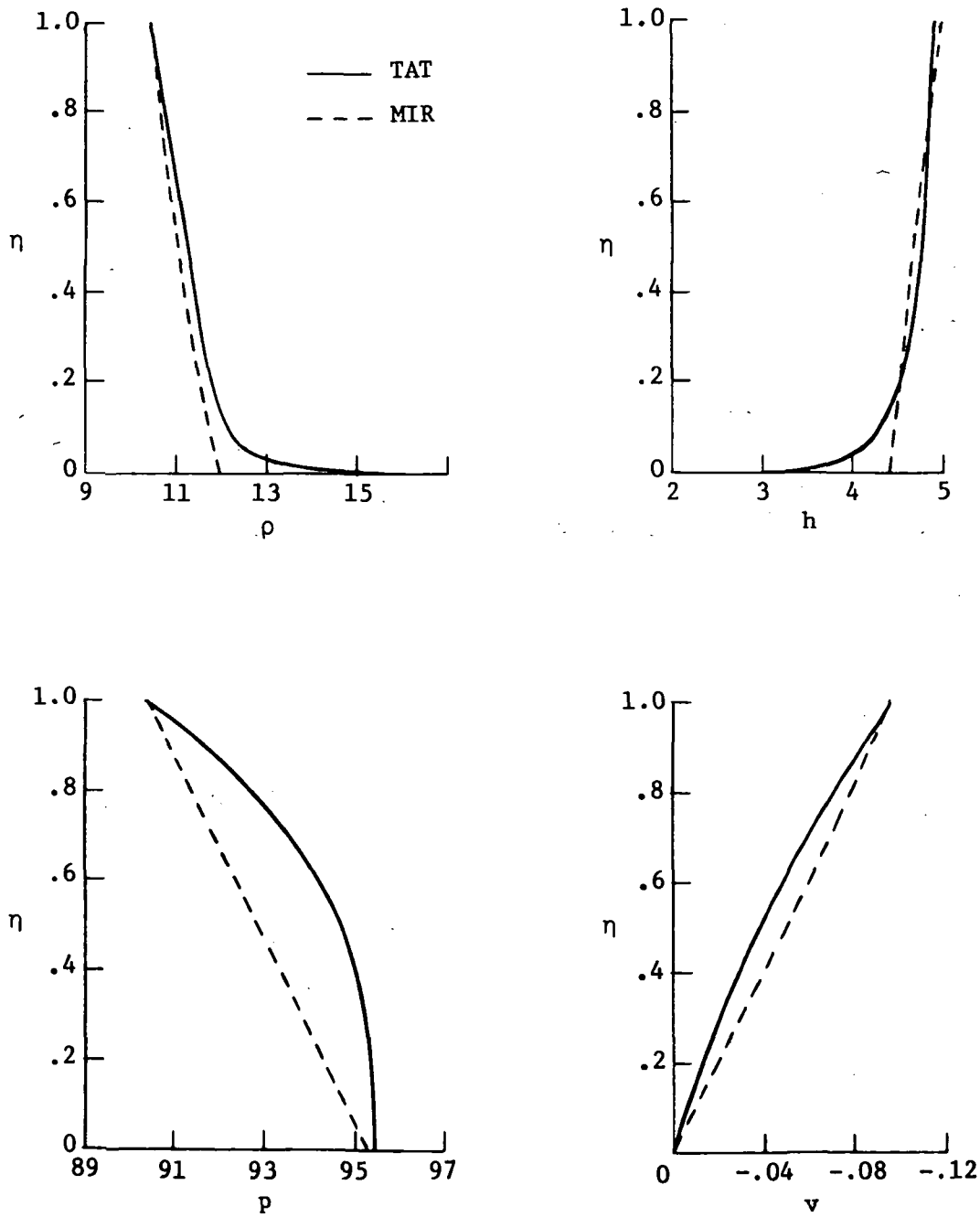

(a) s = 0.

Figure 13.- Shock layer profile properties for Case IV. $\theta_c = 60^o$; $R_N/r_B = 0.5$; and $R_N^* = 0.223$ m.

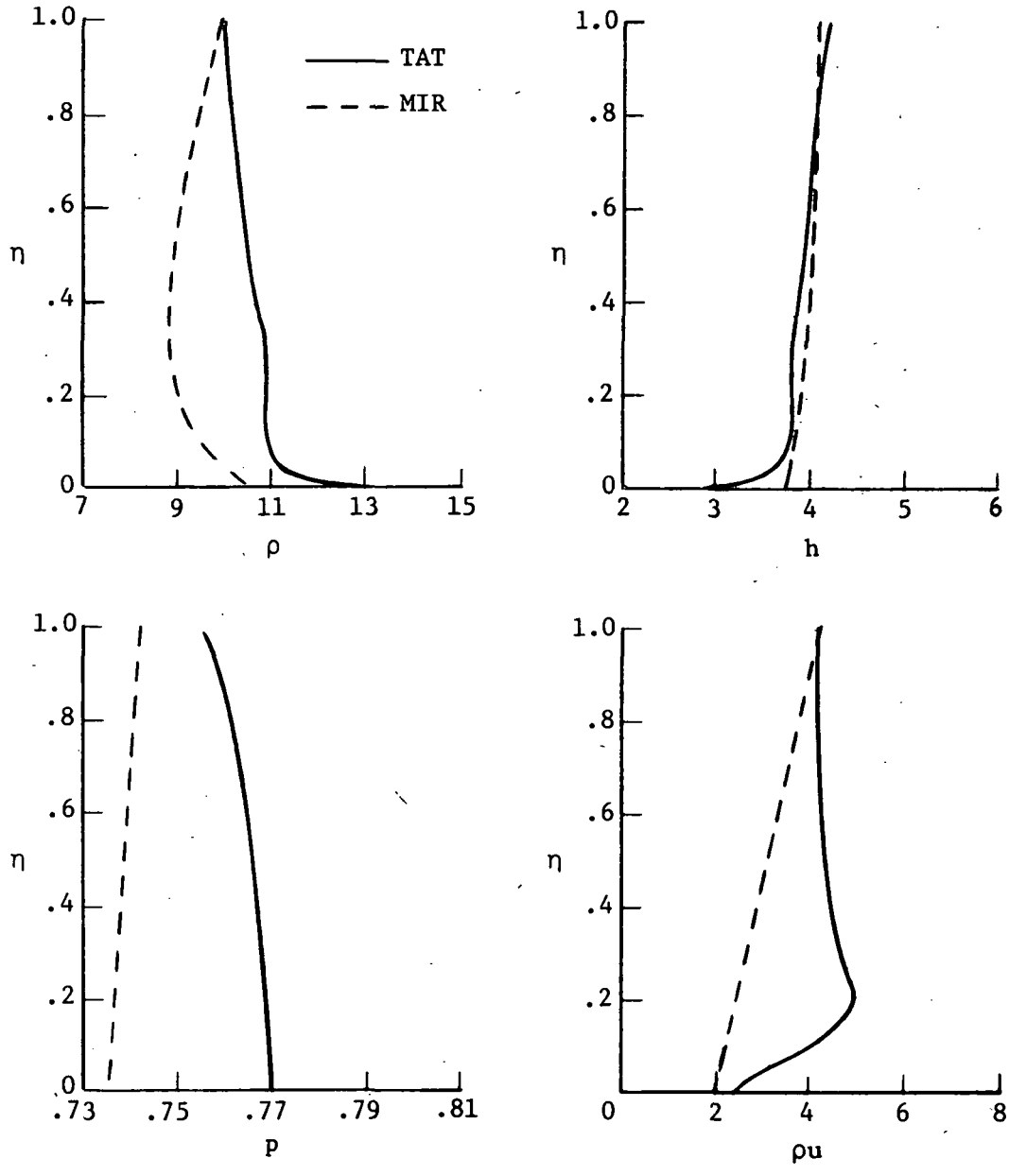

(b) s = 1.8.

Figure 13.- Concluded.

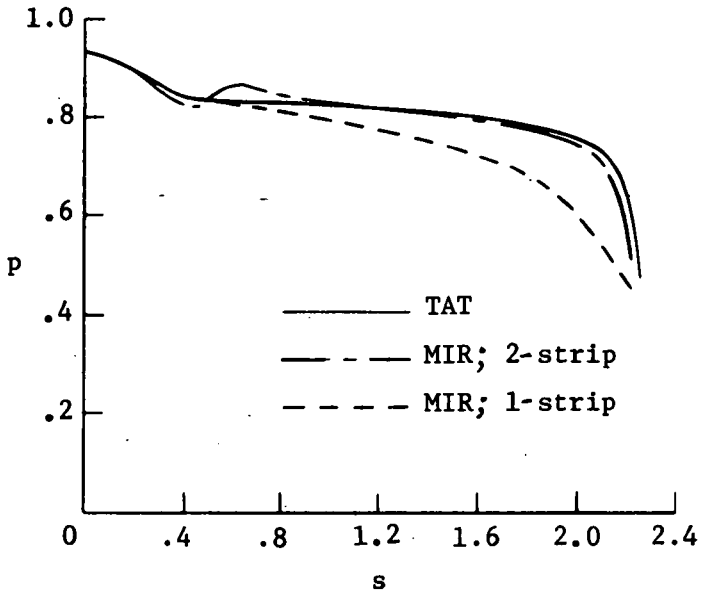

(a) Pressure distribution.

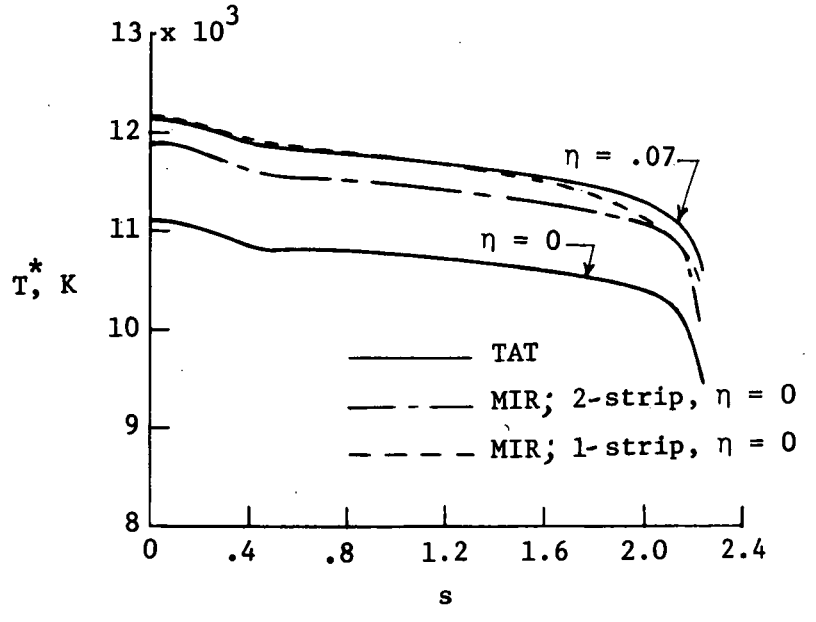

(b) Temperature distribution.

Figure 14.- Comparison of nonadiabatic results for Case V. $\theta_c = 62°$; $R_N/r_B = 0.5$; and $R_N^* = 0.223$ m.

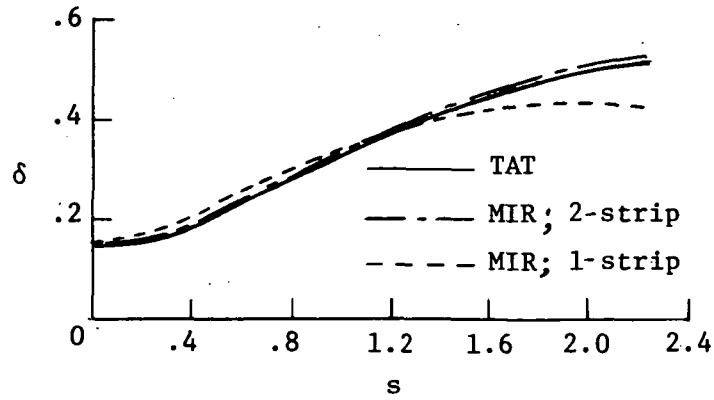

(c) Shock standoff distribution.

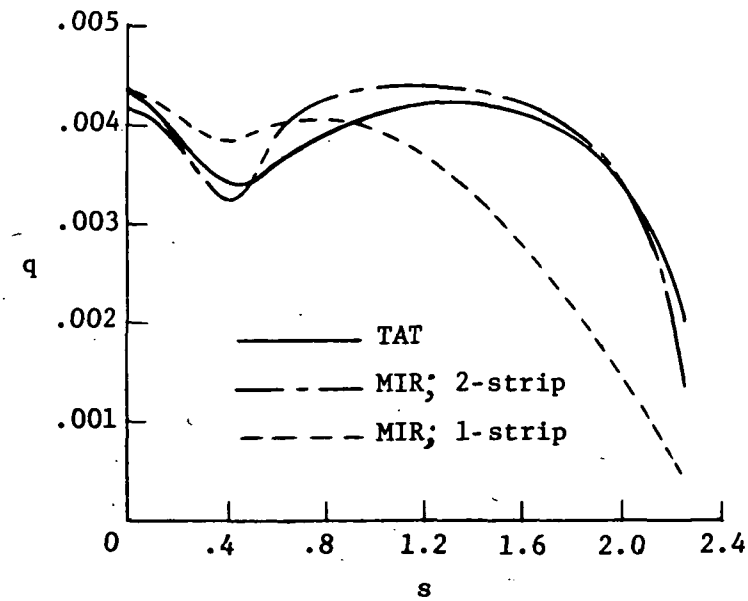

(d) Radiative heating distribution.

Figure 14.- Continued.

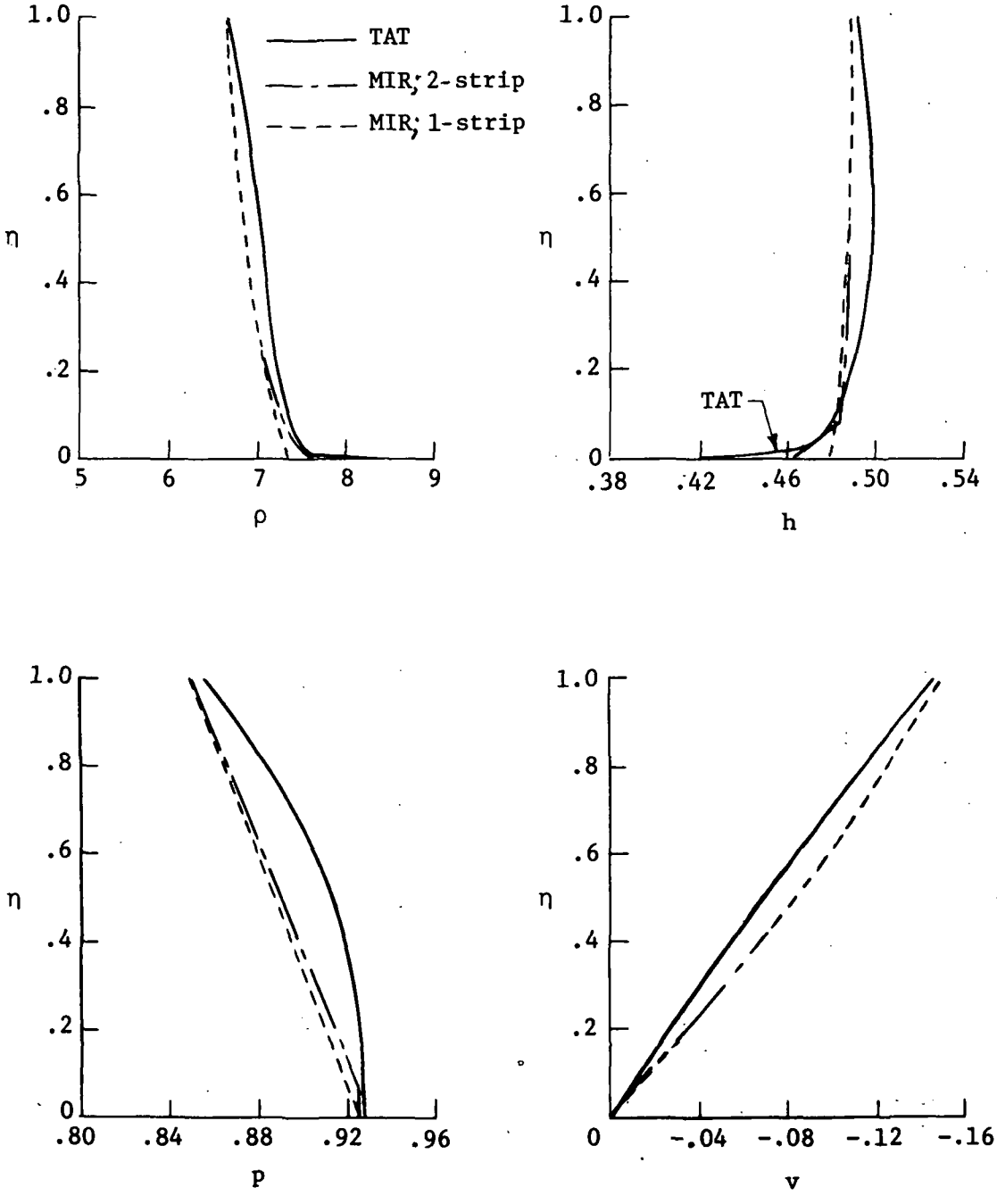

(e) Shock layer profile properties at s = 0.

Figure 14.- Continued.

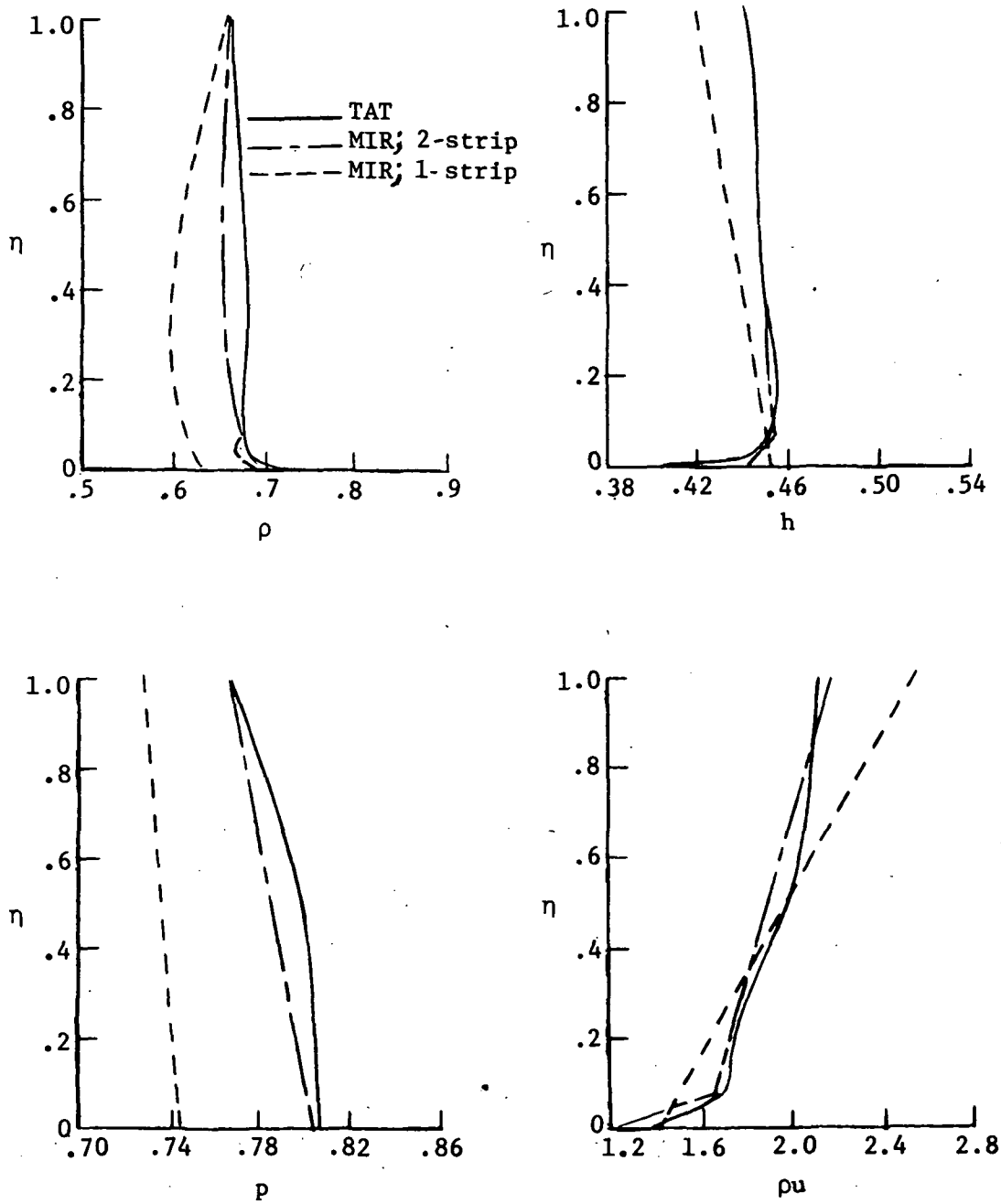

(f) Shock layer profile properties at s = 1.5.

Figure 14.- Concluded.

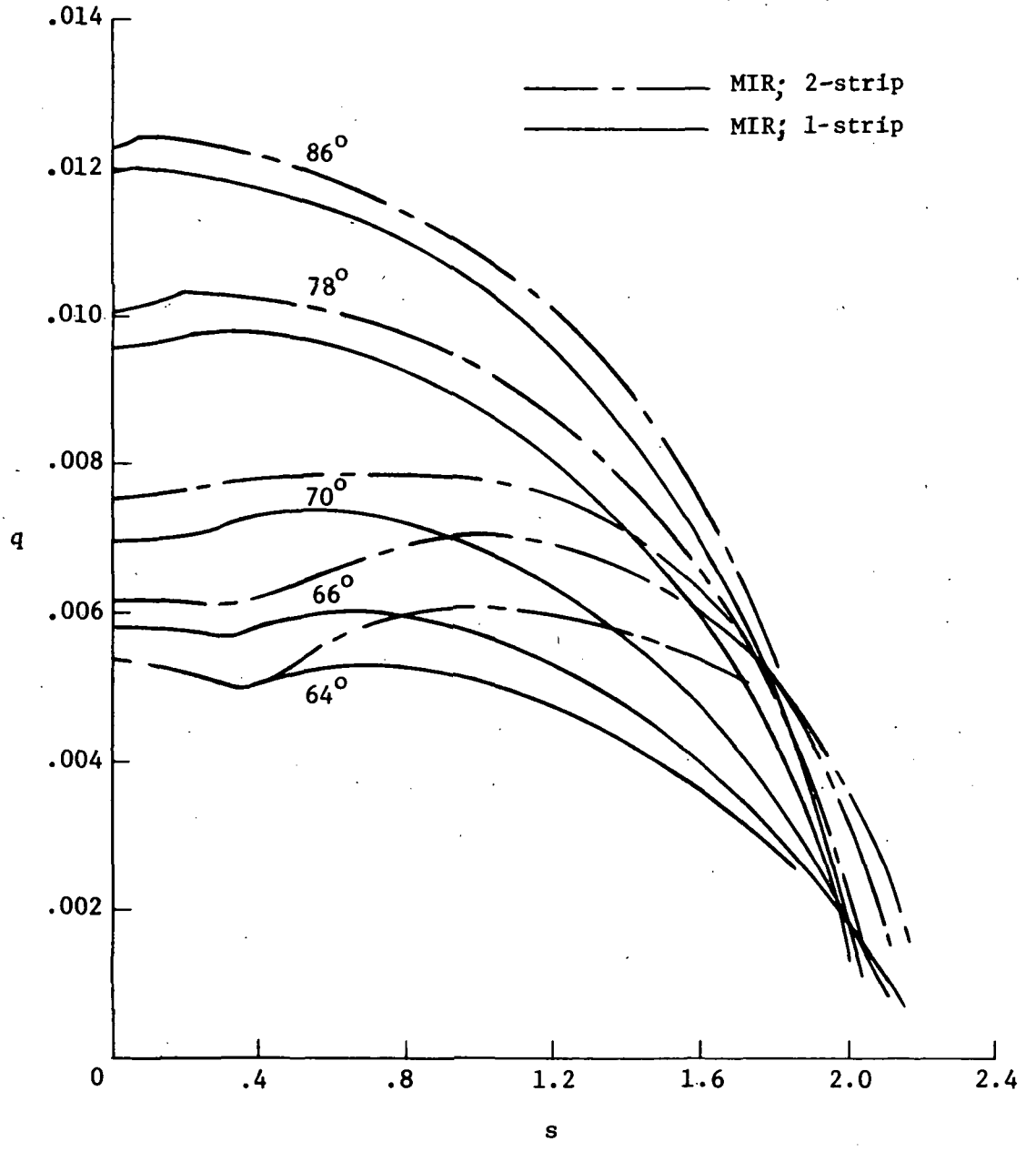

Figure 15.- Effect of cone angle on radiative heat transfer for case V. R_N/r_B = 0.5; and R_N^* = 0.223 m.

1. Report No.	2. Government Accession No.	3. Recipient's Catalog No.
NASA TP-1133		

4. Title and Subtitle	5. Report Date
INVISCID, NONADIABATIC FLOW FIELDS OVER BLUNT, SONIC CORNER BODIES FOR OUTER PLANET ENTRY CONDITIONS BY A METHOD OF INTEGRAL RELATIONS	February 1978
	6. Performing Organization Code

7. Author(s)	8. Performing Organization Report No.
Peter A. Gnoffo	L-11944
	10. Work Unit No. 506-26-10-01
9. Performing Organization Name and Address NASA Langley Research Center Hampton, VA 23665	11. Contract or Grant No.
	13. Type of Report and Period Covered Technical Paper
12. Sponsoring Agency Name and Address National Aeronautics and Space Administration Washington, DC 20546	14. Sponsoring Agency Code

15. Supplementary Notes

16. Abstract

An investigation has been made into the ability of a method of integral relations to calculate inviscid 0° angle of attack, radiative heating distributions over blunt, sonic corner bodies for some representative outer planet entry conditions. Comparisons have been made with a more detailed numerical method, a time asymptotic technique, using the same equilibrium chemistry and radiation transport subroutines. An effort to produce a second-order approximation (two-strip) method of integral relations code to aid in this investigation is also described and a modified two-strip routine is presented. Results indicate that the one-strip method of integral relations cannot be used to obtain accurate estimates of the radiative heating distribution because of its inability to resolve thermal gradients near the wall. The two-strip method can sometimes be used to improve these estimates; however, the two-strip method has only a small range of conditions over which it will yield significant improvement over the one-strip method.

17. Key Words (Suggested by Author(s))	18. Distribution Statement
Method of integral relations Radiative heating Blunt body	Unclassified - Unlimited Subject Category 34

19. Security Classif. (of this report)	20. Security Classif. (of this page)	21. No. of Pages	22. Price*
Unclassified	Unclassified	49	$4.50

* For sale by the National Technical Information Service, Springfield, Virginia 22161

NASA-Langley, 1978

National Aeronautics and
Space Administration

Washington, D.C.
20546

Official Business
Penalty for Private Use, $300

THIRD-CLASS BULK RATE

Postage and Fees Paid
National Aeronautics and
Space Administration
NASA-451

POSTMASTER: If Undeliverable (Section 158 Postal Manual) Do Not Return